



# Structural and functional analysis of the roles of influenza C virus membrane proteins in assembly and budding

Received for publication, November 12, 2021, and in revised form, February 1, 2022. Published, Papers in Press, February 12, 2022, <https://doi.org/10.1016/j.jbc.2022.101727>

Xu Zhang<sup>1,2</sup>, Tim Abel<sup>3</sup>, Shuo Su<sup>1,\*</sup>, Andreas Herrmann<sup>3,4</sup> , Kai Ludwig<sup>5</sup>, and Michael Veit<sup>2,\*</sup>

From the <sup>1</sup>MOE Joint International Research Laboratory of Animal Health and Food Safety, Engineering Laboratory of Animal Immunity of Jiangsu Province, College of Veterinary Medicine, Nanjing Agricultural University, Nanjing, China; <sup>2</sup>Institut für Virologie, Freie Universität Berlin, Berlin, Germany; <sup>3</sup>Institut für Biologie/Molekulare Biophysik, Humboldt-Universität zu Berlin, Berlin, Germany; <sup>4</sup>Biophysikalische Chemie, Institut für Chemie und Biochemie, Freie Universität Berlin, Berlin, Germany; <sup>5</sup>Department of Chemistry and Biochemistry and Core Facility BioSupraMol, Research Center of Electron Microscopy, Free University Berlin, Berlin, Germany

Edited by Craig Cameron

Assembly and budding of the influenza C virus is mediated by three membrane proteins: the hemagglutinin-esterase-fusion glycoprotein (HEF), the matrix protein (CM1), and the ion channel (CM2). Here we investigated whether the formation of the hexagonal HEF arrangement, a distinctive feature of influenza C virions is important for virus budding. We used super resolution microscopy and found 250-nm sized HEF clusters at the plasma membrane of transfected cells, which were insensitive to cholesterol extraction and cytochalasin treatment. Overexpression of either CM1, CM2, or HEF caused the release of membrane-enveloped particles. Cryo-electron microscopy of the latter revealed spherical vesicles exhibiting the hexagonal HEF clusters. We subsequently used reverse genetics to identify elements in HEF required for this clustering. We found that deletion of the short cytoplasmic tail of HEF reduced virus titer and hexagonal HEF arrays, suggesting that an interaction with CM1 stabilizes the HEF clusters. In addition, we substituted amino acids at the surface of the closed HEF conformation and identified specific mutations that prevented virus rescue, others reduced virus titers and the number of HEF clusters in virions. Finally, mutation of two regions that mediate contacts between trimers in the *in-situ* structure of HEF was shown to prevent rescue of infectious virus particles. Mutations at residues thought to mediate lateral interactions were revealed to promote intracellular trafficking defects. Taken together, we propose that lateral interactions between the ectodomains of HEF trimers are a driving force for virus budding, although CM2 and CM1 also play important roles in this process.

Influenza C virus (Flu C) causes flu-like disease but typically only with mild symptoms. The virus has a worldwide distribution, and the majority of humans develop antibodies against the virus early in life (1). Humans are the main reservoir of Flu C, but the virus occasionally infects pigs (2).

Influenza D virus (Flu D) was isolated from clinically ill pigs, but it subsequently turned out that the virus can also infect ferrets, small ruminants, and cattle, which apparently are its main reservoir (3, 4).

Flu C and Flu D are unique among the Orthomyxoviridae since they contain only one spike protein, the hemagglutinin-esterase-fusion glycoprotein (HEF) that possesses receptor binding, receptor destroying, and membrane fusion activities, thus combining the functions of hemagglutinin (HA) and neuraminidase (NA) of Flu A and Flu B viruses (5–7). However, the receptor determinant on the target cell is not acetyl-N-acetylneuraminic acid but an acetylated derivative, namely 9-O-acetyl-N-acetylneuraminic acid (8). Accordingly, to perform the receptor destroying function, HEF does not cleave the terminal neuraminic acid residue from carbohydrates but has an esterase activity that removes acetyl from 9-O-Acetyl-N-acetylneuraminic acid (9). HEF of Flu C and Flu D are stable in evolution, only a few amino acid residues (~5%) are not conserved through all lineages of HEF, which is different to the highly variable HAs of Flu A and Flu B.

Electron microscopy revealed another unique feature of Flu C (and recently of Flu D (10)) particles not observed for Flu A and Flu B virions. The surface of virus particles is covered with a regular network of HEF trimers that has been described to consist mainly of hexagons (11, 12).

HEF (like HA) is a typical type 1 transmembrane protein with a short N-terminal, cleavable signal peptide, a long ectodomain, a transmembrane region, and a very short cytoplasmic tail (Cys-Arg-Thr-Lys). HEF is synthesized as the precursor HEF0, that is cleaved into the N-terminal HEF1 subunit carrying the receptor binding and esterase domain and the membrane-anchored HEF2 subunit which harbors the fusion machinery including the N-terminal hydrophobic fusion peptide (6, 7). Although there is only 12% amino acid identity between HA and HEF, crystallography of their ectodomains revealed that the overall structures as well as folds of individual segments are quite similar (13). HEF of Flu C and Flu D have 55% amino acid identity and an almost identical structural fold (14). HA and HEF form a mushroom-shaped

\* For correspondence: Shuo Su, [shuosu@njau.edu.cn](mailto:shuosu@njau.edu.cn); Michael Veit, [mveit@zedat.fu-berlin.de](mailto:mveit@zedat.fu-berlin.de).

## Influenza C virus budding

trimer consisting of a membrane-near stalk (containing the regions involved in membrane fusion) and a globular head domain carrying the receptor-binding site. HEF contains an additional bulge located at the lower part of the globular domain that carries the esterase region that is not present in HA (13). Very recently, the *in-situ* structure of HEF in virus particles was determined by cryo-electron microscopy (cryo-EM), which revealed a remarkable difference to the structure of the isolated ectodomain. The HEF1 head region is rotated 20° clockwise thereby creating a more open conformation (15), which resembles an early dilated HA fusion intermediate (16). The structure also identified putative contact sites between trimers that might mediate HEF clustering (15). Which function the lateral interactions serve for virus replication has not been investigated. Here we hypothesized that the formation of hexagonal HEF arrays is required for virus assembly and budding.

Virus budding can be divided into several steps (17–19). The first step is transport of viral components to the budding site. Viral proteins might have intrinsic signals that target them to the plasma membrane, or they are recruited by other viral proteins, such as the ion channel protein M2 of Flu A, which binds to the matrix protein M1 at the Golgi complex and carries it by a piggy-back mechanism to the plasma membrane (20). The second step is the assembly of viral components, which is mediated by interactions between viral proteins that exclude most cellular proteins from the budding site. Virus assembly might be preceded by clustering of viral glycoproteins in cholesterol-enriched nanodomains of the plasma membrane that might be stabilized by the cytoskeleton (21, 22). Alternatively, or in addition, lateral interactions between the ectodomains of viral glycoproteins could in principle also lead to clustering. After assembly, the budding process itself needs an element which physically drives membrane bending to generate a  $\Omega$ -shaped bud. During the budding process, a part of the (almost) planar plasma membrane is converted into a spherical, thus highly curved envelope. Since the plasma membrane tends to stay flat, this shape change is an energetically unfavorable process, and the required energy must be provided by interactions with proteins (19). In principle, protein oligomers attached to the inner leaflet of the membrane can provide “scaffolding” that leads to membrane bending. If these initially flat clusters recruit more and more proteins, they are transformed into a curved structure and finally into a sphere and such an internal coat provides a pushing force for virus budding. An example is M1 of Flu A when it is co-expressed with M2 or NA (20, 23). Membrane bending might also occur by oligomerization of an external coat. This principle is often realized in vesicular transport of the cell, *e.g.*, in formation of COPI and COPII vesicles (24), and in budding of flaviviruses, where coat formation executes a pulling force onto the membrane (25). A modification of the external coat idea is the “crowding hypothesis”, *i.e.*, a high concentration of a protein, especially if it is cone-shaped like a viral spike protein, might induce membrane curvature without forming lateral interactions (26). Finally, membrane bending can also be induced by amphiphilic helices which insert into

the inner leaflet of the plasma membrane. The helix can act as a “wedge” by displacing membrane lipids in only one bilayer leaflet that locally induces membrane curvature (27). This has been shown for M2 of Flu A which localizes to the edge of the viral budzone to mediate pinching-off of virus particles (28).

Very little is known about assembly and budding of Flu C. Besides HEF, Flu C encodes only two other membrane proteins. CM2 is a short tetrameric integral membrane glycoprotein structurally analogous to Flu A M2 (29). Like M2, CM2 is supposed to exhibit proton-channel activity required for virus entry (30). Whether CM2 plays a role for release of Flu C as described for M2 of Flu A has not been investigated. The matrix protein CM1, a peripheral membrane protein, covers the viral envelope on its inside. The 3D structures of the N-terminal domain of CM1 and M1 from Flu A are very similar, despite the low sequence similarity (31). CM1 has been shown to induce the formation of protrusions, called cord-like structures, emanating out of infected cells and regulating their growth, thus demonstrating a role for CM1 in membrane remodeling (32, 33). Furthermore, purified CM1 binds to negatively charged artificial membranes (giant unilamellar vesicles [GUVs]) and induces tubular membrane invaginations suggesting that CM1 might execute a pushing force by oligomerization at the inner site of the plasma membrane (31). However, it is not known whether CM1 is intrinsically targeted to the plasma membrane and how the functions of HEF and CM1 are coupled. HEF contains only a very short cytoplasmic tail (RTK in Flu C and KK in Flu D) that is unlikely to make extensive contacts with CM1. Likewise, it was never investigated whether expression of CM1 (or any of the other membrane proteins of Flu C) causes the formation of virus-like particles (VLPs), membranous vesicles, or filaments which are released from cells expressing viral membrane proteins. Release of membranous protein particles is generally seen as evidence that a certain viral protein (or a combination) can cause membrane curvature and vesiculation and is thus considered as the driving force for virus budding.

Here, we expressed Flu C membrane proteins from a plasmid to study their trafficking inside cells by confocal microscopy and cluster formation of HEF by super resolution microscopy. It was then investigated biochemically which proteins are able to release protein particles, and their morphology was studied by cryo-EM. Next, we exchanged amino acids supposed to mediate interactions between HEF trimers both in the closed and open HEF conformation to investigate their effect on virus replication and particle formation. The results are compared with those of similar experiments published for membrane proteins of Flu A to reveal common and different principles of budding among influenza virus genera.

## Results

### Localization of HEF, CM1, and CM2 in transfected cells

We first investigated the intracellular localization of HEF, CM1, and CM2 in transfected Chinese hamster ovary cells (CHO-K1) cells using confocal microscopy. For visualization

of HEF, we used a polyclonal antiserum against the glycoprotein, whereas CM1 and CM2 were equipped with a C-terminal His-tag and HA-tag, respectively. All three proteins, if expressed alone, are present mainly at or near the plasma membrane, but especially HEF and CM1 are not uniformly distributed but are enriched in certain membrane areas (Fig. 1A). Cells expressing HEF or CM1 also revealed long filaments protruding from the cell surface that contain punctate fluorescence (marked with *arrowhead* and magnified in some figures). Remarkably, not a single cell showed CM1 in the nucleus, which is in contrast to M1 of Flu A (34, 35). Cells expressing CM2 revealed no visible extensions at the cell surface. In comparison to CM1 and HEF, a stronger fluorescence signal was detected for CM2 inside cells, which likely represents organelles of the exocytic pathway (endoplasmic reticulum [ER] and Golgi complex), which are used by CM2 and also HEF for transport to the plasma membrane. To explore whether CM1, which has no signal peptide for ER targeting, uses the same pathway for surface transport or binds

directly to the plasma membrane, CM1-expressing cells were costained with antibodies labeling either the ER, the cis-Golgi region (anti-GM130), or the whole Golgi apparatus (anti-58K protein). No overlap was detected with the ER marker and the cis-Golgi marker, which stains a perinuclear region of the Golgi (Fig. 1B). However, CM1 clearly colocalizes with the 58k-protein Golgi marker in a more distal cellular region. This suggests that at least a fraction of CM1 attaches to distal cisternae of the Golgi complex using subsequently the exocytic pathway for transport to the plasma membrane.

Next, we co-expressed the membrane proteins in all possible combinations and quantified the degree of colocalization of two fluorophores using Pearson's correlation coefficient (Fig. 1, C–E). The highest level of colocalization (~80%, mean of three transfection experiments) were calculated for HEF and CM1, regardless of whether both proteins were co-expressed (Fig. 1D) or CM2 was expressed in addition (Fig. 1E). Around 70% of HEF and CM2 molecules colocalize in double and 50% in triple transfected cells, but the results are

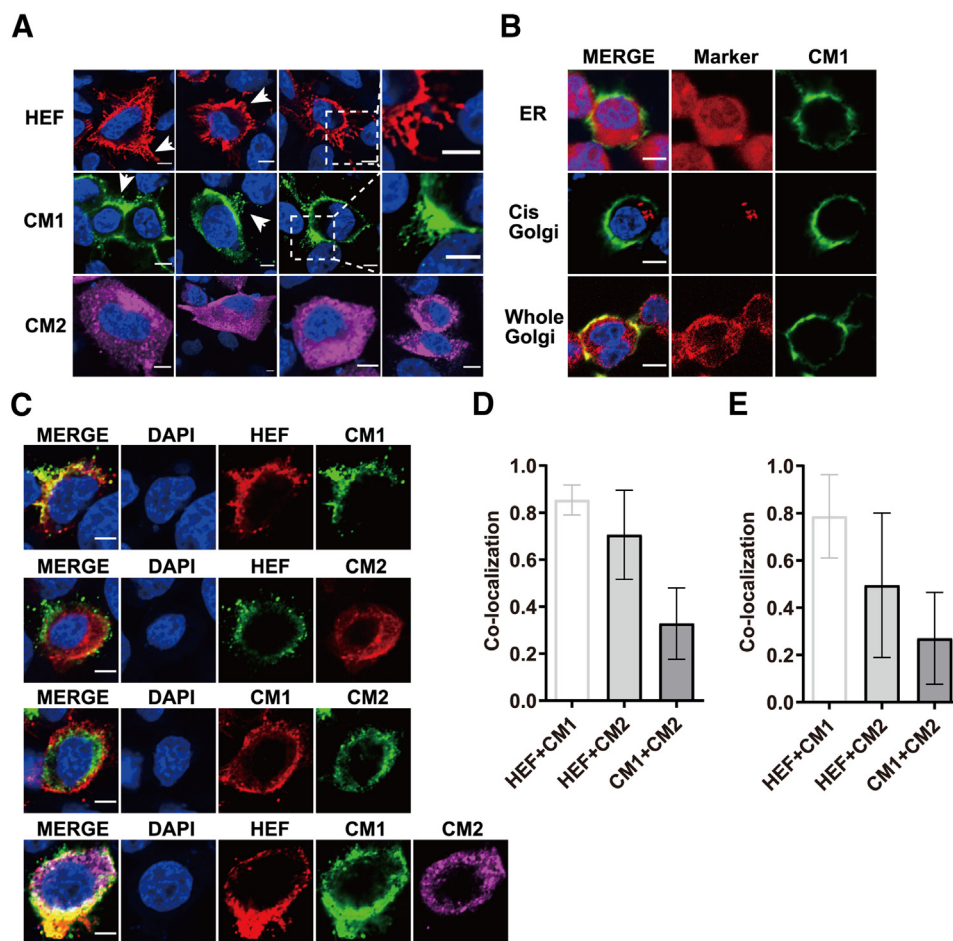


**Figure 1. Localization of HEF, CM1, and CM2 in transfected cells.** A, fluorescence micrographs of CHO-K1 cells transfected with expression plasmids encoding HEF, CM1-His, and CM2-HA. Cells were fixed, permeabilized, and labeled with anti-HEF (red), anti-His (green), and anti-HA (magenta) and suitable secondary antibodies at 24 h posttransfection. Nuclei were stained with DAPI. Surface projections in cells expressing HEF and CM1-His are marked with an *arrowhead* and magnified in the *right image*. Scale bar: 5  $\mu$ m. B, colocalization of CM1-His with ER marker, cis-Golgi marker GM130, and whole Golgi marker anti-58K protein. Scale bar: 5  $\mu$ m. C, colocalization of HEF, CM1-His, and CM2-HA in double or triple transfected CHO-K1 cells. Scale bar: 5  $\mu$ m. D, quantitative analysis of colocalization in cells double transfected with the indicated plasmids. E, quantitative analysis of colocalization of the indicated proteins in cells co-expressing HEF, CM1-His, and CM2-HA. Colocalization was quantified from at least 40 cells with the Pearson's correlation coefficient method using the JACoP plugin of the ImageJ software. CHO-K1, Chinese hamster ovary cells; ER, endoplasmic reticulum; HA, hemagglutinin; HEF, hemagglutinin-esterase-fusion glycoprotein.

## Influenza C virus budding

not statistically significant different from each other. The lowest levels of colocalization were observed between CM1 and CM2, ~30% both in double and in triple transfected cells. We conclude that all Flu C membrane proteins are intrinsically targeted to the plasma membrane, the viral budding site, where they colocalize to a varying extent.

### Super resolution microscopy revealed clustering of HEF

We further investigated the HEF accumulations by super resolution microscopy. Since the diameter of influenza viruses (approx. 120 nm) is below the resolution limit of conventional fluorescence microscopy, clustering of HEF was assessed by direct stochastic optical reconstruction microscopy

(dSTORM) using a homebuilt widefield microscope. dSTORM-imaging does not only allow a more robust assessment of the cluster diameters, but also, since blinking events are proportional to the number of fluorophores present, can estimate the number of molecules assembled in clusters. To investigate possible differences between HEF expressed alone and in the context of a virus infection, we used polarized Madin-Darby canine kidney cells, subline I (MDCK I) cells for our analysis. For visualization of HEF, we used an anti-HEF antibody in combination with a corresponding secondary antibody coupled to Alexa Fluor 647. To exclude that clusters are formed by antibody-mediated crosslinking of HEF trimers, cells were fixed prior to antibody treatment. [Figure 2B](#) shows a confocal widefield image, and [Figure 2C](#) shows the

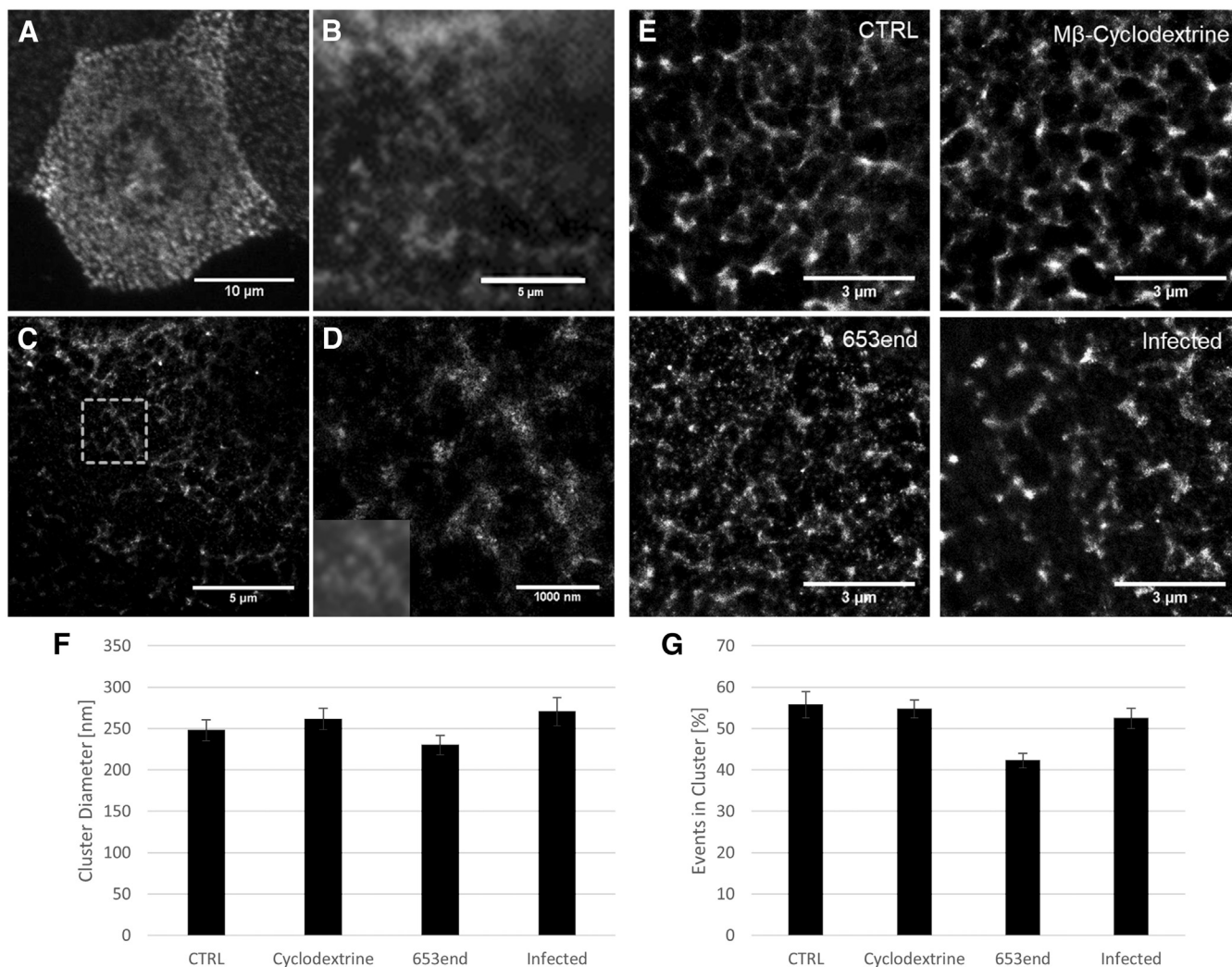


**Figure 2. dSTORM super resolution fluorescence microscopy reveals HEF clusters in MDCK I cells.** Lateral organization of HEF on the apical plasma membrane of unpermeabilized, fixed MDCK I cells imaged by different techniques. *A*, maximum intensity projection of a z-stack from confocal images, *(B)* Wide field image, *(C)* dSTORM image of the same area as in *(B)*, *(D)* enlargement of the area marked in *(C)*. *Inset in lower, left corner*, the same field of view of *(D)* is shown in the wide-field image, which is reduced about 10-fold compared to the STORM image. *E*, representative dSTORM images of WT HEF (CTRL), WT HEF after cholesterol extraction (Mβ-cyclodextrin), HEF missing its cytosolic domain (653End) and cells infected with influenza C virus (infected). Except for the latter, all the other experiments were performed with transfected cells. *F*, Voronoi tessellation-based quantitative analysis of the impact of the different treatments on the average cluster diameter and *(G)* the percentage of HEF localization events in clusters. Only accumulations larger than 100 nm were regarded as clusters.  $n = 5$  (CTRL, control),  $n = 7$  (Mβ-cyclodextrin treated),  $n = 4$  (653End), and  $n = 7$  (infected). Images were taken from the apical membrane of fixed, polarized MDCK I cells 24 h after transfection and subsequent immunohistochemical labeling with anti-HEF antibodies and secondary antibodies coupled to the fluorophore Alexa Fluor-647. Mutant 653end was significantly ( $p = 0.005$ ) less organized in clusters. dSTORM, direct stochastic optical reconstruction microscopy; HEF, hemagglutinin-esterase-fusion glycoprotein; MDCK I, Madin-Darby canine kidney cells, subline I.

corresponding dSTORM image of the apical membrane of a transfected MDCK I cell (Fig. 2A) demonstrating the difference in resolution. Upon further magnification of the dSTORM image reticular HEF clusters were visible, which were formed from partially overlapping accumulations with an extension of several hundred nanometers (Fig. 2C). The optical resolution was estimated to be  $\approx 50$  nm using Fourier ring correlation.

A quantitative Voronoi tessellation analysis (36) estimated that around 55% of HEF trimers are clustered and calculated an average diameter of about 250 nm for the HEF clusters (Fig. 2F). This size corresponds to the surface area of a sphere with a diameter of 150 nm and therefore to the surface area required for virus budding. Using the same analysis, we asked whether similar HEF clusters are present in the apical membrane of infected MDCK I cells (Fig. 2E). The mean cluster diameter and the fraction of HEF organized in clusters were comparable between infected and transfected cells, indicating that HEF-cluster formation is independent of other virus components.

Next, we considered whether host components might cause clustering of HEF. HA of Flu A is clustered by association with cholesterol-enriched nanodomains of the plasma membrane, which might be stabilized by elements of the cytoskeleton, especially cortical actin filaments (21, 22). Therefore, transfected MDCK I cells were treated for 1 h prior to fixation with either cytochalasin (1  $\mu$ M), which prevents polymerization of actin or with methyl- $\beta$ -cyclodextrin (5 mM) that extracts cholesterol from the plasma membrane. The mean cluster size was not reduced after M $\beta$ -cyclodextrin (Fig. 2E) or cytochalasin (image not shown) treatment, and the fraction of HEF molecules organized in clusters was also not affected. These results strongly suggest that HEF clustering is an intrinsic property of the protein.

#### **Release of protein-containing particles after expression of HEF, CM1, and CM2**

Expression of viral membrane proteins and the subsequent analysis of particulate material in the supernatant has been widely used to determine which of them is able to bend and vesiculate the plasma membrane and hence is the so-called driving force for virus budding. To investigate this, we transfected human embryonic kidney 293T (HEK-293T) cells with expression plasmids encoding HEF, CM1-His, and CM2-HA. Cellular supernatants were harvested at 48 h posttransfection, cleared from cell debris, and centrifuged through a 20% sucrose cushion. The resulting pellet as well as aliquots of cell lysates were subjected to Western blotting with anti-HEF, anti-His, and anti-HA antibodies, respectively. The results show that each protein if expressed alone shed particulate antigen into the supernatant (Fig. 3A). Whereas HEF and CM1 show a single band in the blots, several forms of CM2 with different electrophoretic mobilities were detected. The bands are due to N-glycosylation, as demonstrated by digestion with PNGase-F. As previously described, the CM2 bands consist of an

unglycosylated (MW 16 kDa) and a mannose-rich precursor (MW 18 kDa) which are processed into a heterogeneously glycosylated product (MW 22–30 kDa) (37).

We also asked whether more protein particles are released into the supernatant if the membrane proteins are co-expressed, as described for Flu A (38). The transfection experiment was performed five times, band densities were determined, and the ratio of released protein relative to its expression level was calculated. The value for each sample was normalized to that obtained when the protein was expressed alone. When HEF and CM1 were co-expressed or together with CM2, the amount of protein particles released into the supernatant did not increase in a significant manner (Fig. 3, B–D). In contrast, release of CM2 was significantly reduced to 20% if co-expressed with HEF or with HEF and CM1 and slightly but statistically insignificant if co-expressed with CM1. Note, however, that we observed considerable variation between experiments, especially regarding the amount of CM2 if co-expressed with HEF. In three experiment, CM2 was detected in the supernatant only after long exposure of the blot, but in the other two experiments, it was more readily detectable.

To determine the morphology of the released material, especially whether they are composed of aggregated proteins or proteins embedded in a membrane, we examined the cellular supernatants after sedimentation through a 20% sucrose cushion by negative staining electron microscopy using 1% phosphotungstic acid adjusted to pH 7.4 as contrasting agent. The supernatant from HEF-expressing cells shows membranous vesicles with protein clusters building the typical hexagonal arrays. They are enriched in some areas of the vesicle, where they form structures resembling various stages of virus budding (Fig. 4). Material from the supernatant of CM1-expressing cells exhibits ellipsoid or filamentous vesicles of different sizes. Provided that the staining material penetrated the particles, an internal structure is visible that presumably represents oligomers of CM1. The supernatant from CM2-expressing cells contains very long filaments, and essentially the same structures were seen if CM1 is co-expressed (not shown). If HEF is co-expressed with either CM2 or especially with CM1, the vesicles exhibit hexagonal HEF arrays which cover now (almost) the whole surface of the vesicle. If all three viral proteins are expressed, all types of particles were present, but only in a few cases, some of the membranous particles looked essentially like virus particles (Fig. 4).

In summary, expression of all three membrane proteins of Flu C causes release of membranous protein-containing particles into the supernatant of transfected cells indicating that each of them is able to vesiculate membranes. HEF, if expressed alone, forms hexagonal arrays on the surface of the vesicles which resemble budding virus particles. This indicates that formation of a hexagonal array of HEF clusters is one driving force of virus budding. The amount of membranous protein-containing particles is not increased upon co-expression of two or three membrane proteins. CM2 is

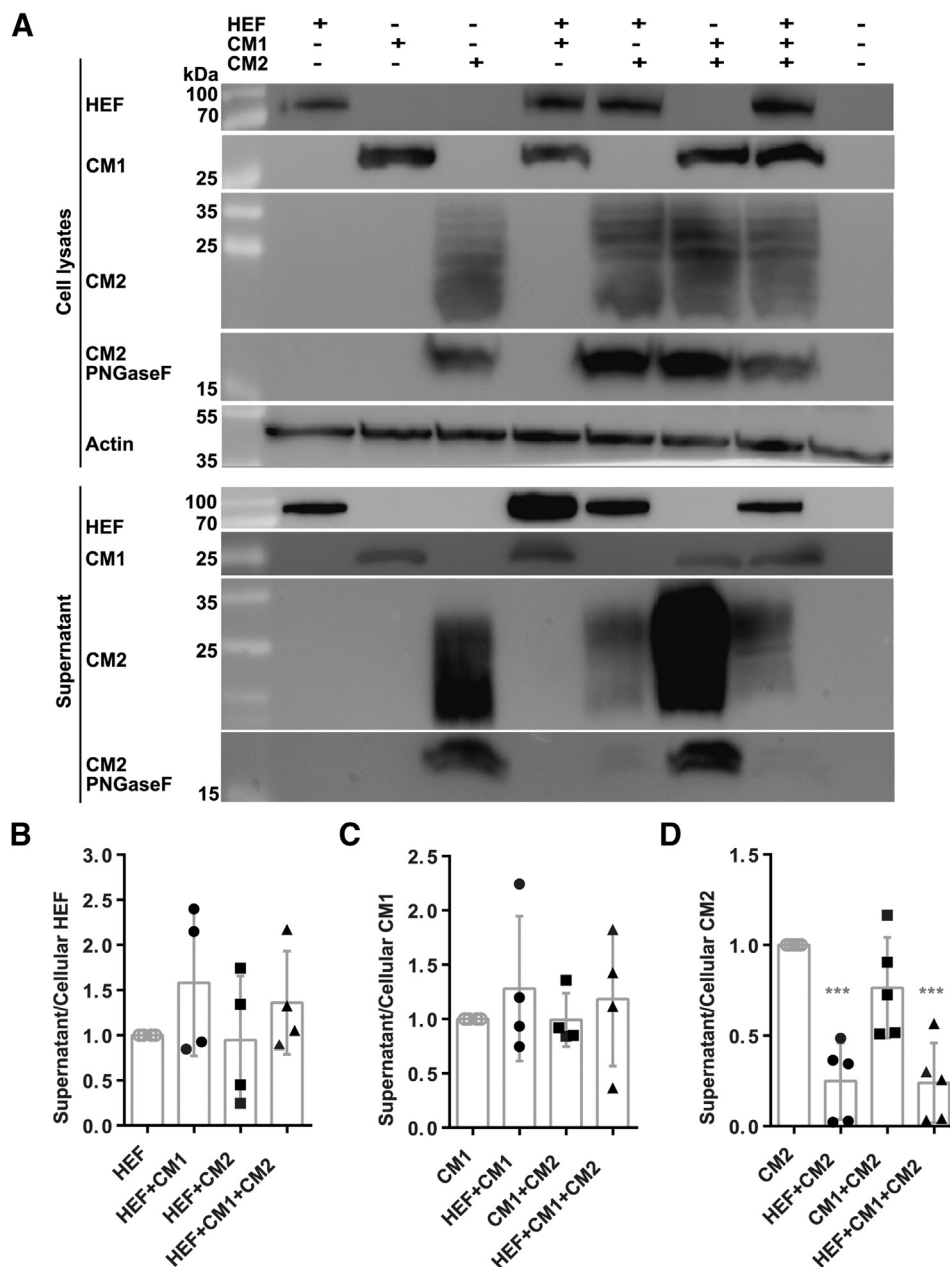


**Figure 3. Release of particles into the supernatant of cells expressing HEF, CM1-His, and CM2-HA.** A, Western blot analysis of supernatants from transfected HEK-293T cells after centrifugation through a 20% sucrose cushion and of the corresponding cell lysates. Cells were transfected with plasmids expressing HEF, CM1-His, and CM2-HA, alone or in the combinations as indicated, and processed at 48 h posttransfection. Anti-actin antibodies were used as a loading control. B, normalized ratio of HEF in the supernatants to HEF in the lysates of cells expressing HEF alone or in combination with CM1 and/or CM2. C, normalized ratio of CM1 in the supernatants to CM1 in the lysates of cells expressing CM1 alone or in combination with HEF and/or CM2. D, normalized ratio of CM2 in the supernatants to CM2 in the lysates of cells expressing CM2 alone or in combination with HEF and/or CM1. One-way ANOVA followed by Tukey's multiple comparison test was applied for statistical analysis of the band densities from four or five transfection experiments. Only CM2 revealed statistically significant differences as indicated by asterisks (\* $p < 0.05$ , \*\* $p < 0.01$ , \*\*\* $p < 0.001$ ). HA, hemagglutinin; HEF, hemagglutinin-esterase-fusion glycoprotein; HEK-293T, human embryonic kidney-293T cells.

apparently partly displaced from the budding site, but it nevertheless affects the morphology of the particles.

#### Exchange of amino acids in the cytoplasmic tail of HEF

In the next set of experiments, we aimed to identify amino acids responsible for HEF clustering. The cytoplasmic tail of HEF might interact with CM1, which forms a dense matrix layer at the inner membrane leaflet where it might

stabilize the HEF clusters. We therefore investigated first whether removal of the very short cytoplasmic tail of HEF (Cys-Arg-Thr-Lys) affects virus replication. We created one mutant where a stop codon was inserted instead of Arg at position 653 and another where it was inserted at position 652 which also removes the S-acylated cysteine located at the end of the transmembrane region (39). HEF plasmids, either WT or the mutants were transfected together with the remaining six plasmids to express all viral proteins in

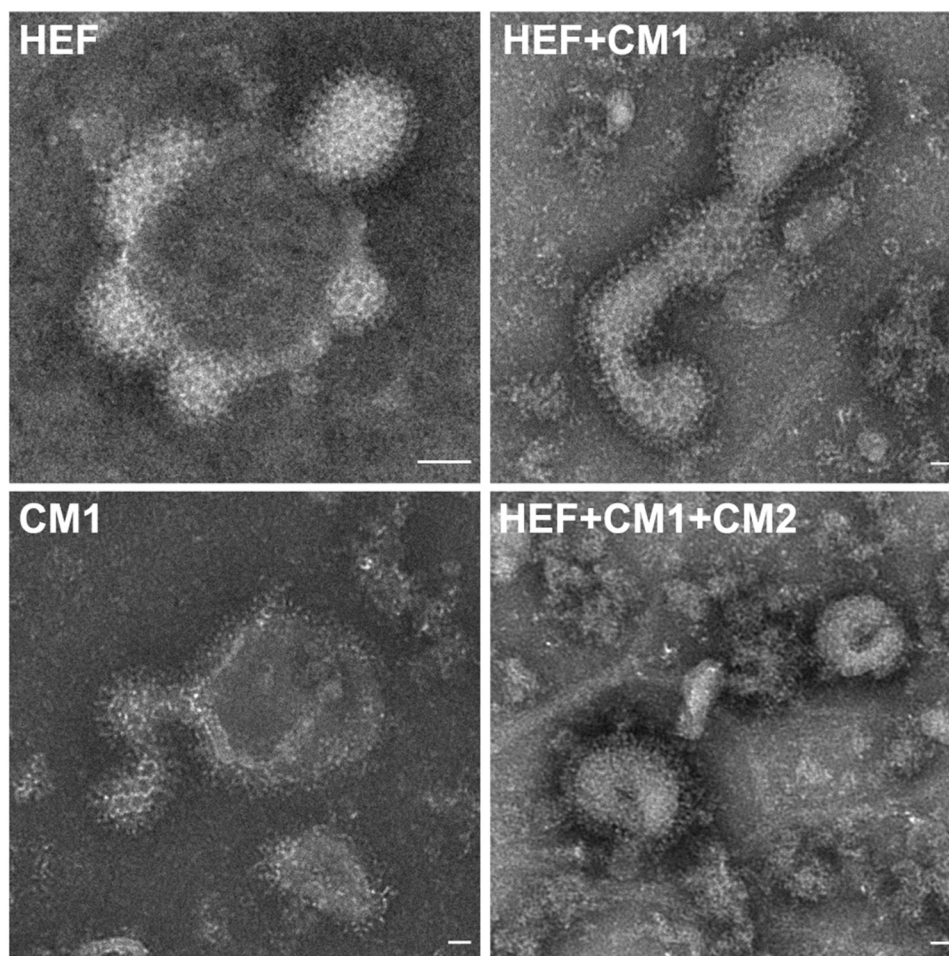


**Figure 4. Negative stain electron microscopy of released particles.** Sections of negative stain micrographs of particles released into the supernatant of transfected HEK-293T cells and pelleted through a 20% sucrose cushion. Cells were transfected with plasmids encoding HEF either alone or together with plasmids encoding CM1 and/or CM2 as indicated. The scale bar corresponds to 500 nm. The respective structures were only observed when the cells were transfected with the indicated plasmids, indicating their specificity. HEF, hemagglutinin-esterase-fusion glycoprotein; HEK-293T, human embryonic kidney-293T cells.

Vero cells, and virus present in the resulting supernatant was further amplified in MDCK I cells. The resulting virus stock was titrated, and the HEF gene sequenced to verify the presence of the mutation. To compare the growth kinetics of the viruses, we infected MDCK I cells at a low multiplicity of infection (MOI) and removed aliquots from cellular supernatants at day 1, 2, 3, 4, 5, 6, and 7 after infection for subsequent tissue culture infective dose (TCID<sub>50</sub>) and HA assays. Both the infection experiments and virus titration were performed at 33 °C, the optimal growth temperature of Flu C (40, 41). Infectious wildtype virus was detected 1 day after infection, and the titer increased by roughly one log each day until the curve flattens out on day 4 (Fig. 5A). HA assays revealed the same kinetics, except that titers increased until day 5 (Fig. 5B). Removal of the cytoplasmic tail (mutant 653End) caused a delay in virus production, and especially infectious virus titers were reduced by one to two logs, statistically significant at day 4 (mean of three growth experiments). When the acylation site was also removed (mutant 652End), the delay in virus growth and the reduction in virus titers were even more pronounced, up to three logs 5 days postinfection. In

our previous study, we reported a one log reduction of the virus titer if only the acylated cysteine site was replaced by a serine (42). The higher reduction in virus titers if the tail plus the acylation site were removed indicates that acylation and the short cytoplasmic tail cooperate synergistically.

To assess whether the mutations affected the specific infectivity of the viruses, we calculated the plaque forming unit (PFU)/HA ratios at 3, 4, 5, and 6 days after infection. The ratio decreased for the WT virus from day 4 to day 6 most likely because virus particles released early in the experiment became already disintegrated. This reduces their infectivity, but not necessarily their ability to hemagglutinate. More importantly, both mutant viruses revealed a reduced specific infectivity compared to WT at all time points. This indicates that the same number of physical (hemagglutinating) particles contain less infectious particles suggesting that the cytoplasmic tail mutants (also) have a defect in virus infection. Accordingly, our previous analysis with the HEF mutant with the acylated cysteine exchanged revealed a small defect in hemolysis, a surrogate marker for membrane fusion whereas the HEF clusters appeared normal (42). Alternatively, or additionally, the mutant viral particles could also have a defect

## Influenza C virus budding

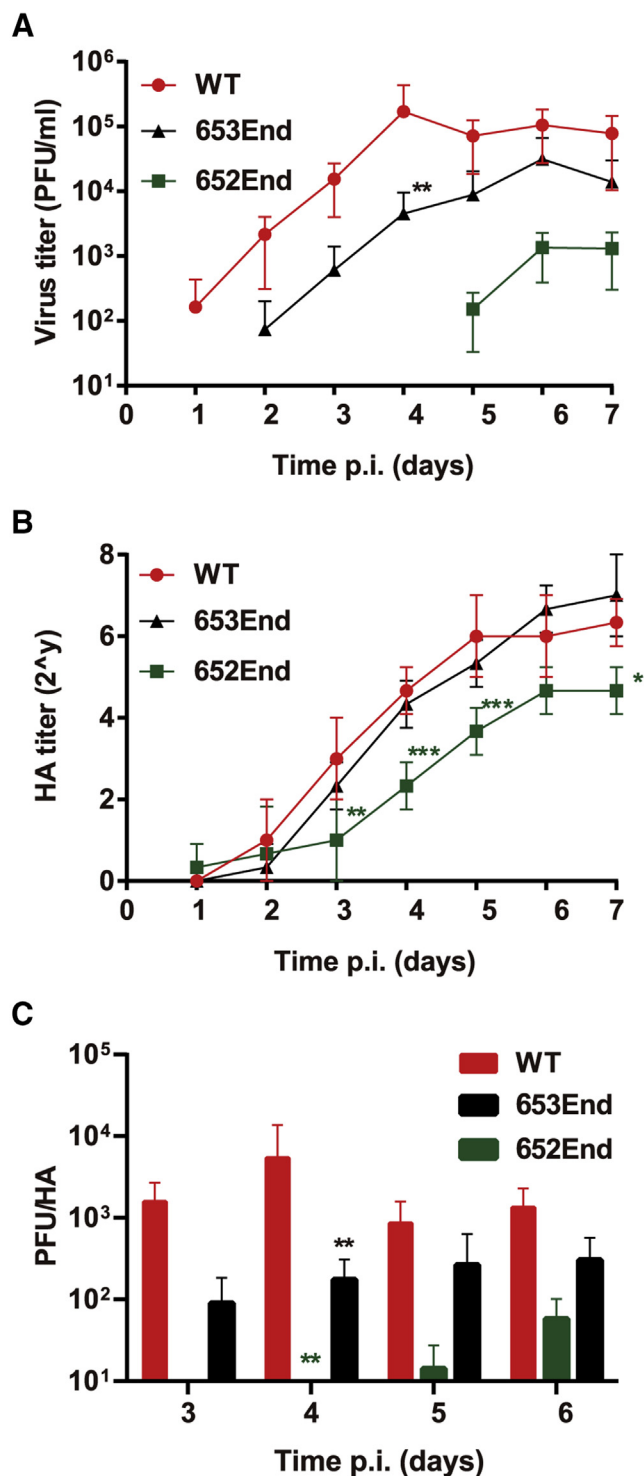


**Figure 5. Growth kinetics of Flu C WT and HEF mutants with deleted cytoplasmic tail.** MDCK I cells in 24-well plates were infected at an MOI of 0.05 with Flu C, WT, or HEF mutants with a stop codon at position 652 or 653. *A* and *B*, culture supernatants were collected at the indicated time points, and titers were determined with a TCID<sub>50</sub> (*A*) or an HA assay (*B*). TCID<sub>50</sub> titers were converted into PFUs. *C*, ratio of PFU to HA titers calculated for the indicated time points. The graphs show the mean titers with standard deviations (error bars) from three independent infections. The asterisks indicate statistically significant differences (\**p* < 0.05, \*\**p* < 0.01, \*\*\**p* < 0.001) between WT and the mutants. One-way ANOVA followed by Tukey's multiple comparison test was applied for statistical analysis. Flu C, influenza C virus; HA, hemagglutinin; HEF, hemagglutinin-esterase-fusion glycoprotein; MDCK I, Madin-Darby canine kidney cells, subline I; PFU, plaque forming unit.

in the correct packaging of the seven viral genome segments, which would also reduce the number of infectious particles.

We next asked whether deletion of the cytoplasmic tail of HEF affects the morphology of virus particles. Since the mutant 652End grows to very low titers, we were only able to prepare the mutant 653End for microscopic analysis. To be able to assess small differences, if any, we wanted to employ cryo-EM to study the viruses under native, hydrated conditions. However, since normal cryo-EM (projection) images did often not clearly resolve the regular HEF arrangements (not shown), we used cryo-electron tomography (cryo-ET) to obtain information on the local 3D structure. Figure 6 shows a slice of a 3D reconstruction of the tomography series of WT Flu C, which revealed a variety of particle shapes. We observed particles completely lacking spike proteins (marked with B, bald), viruses that are only partially covered with HEF spikes (P), and viruses with a dense population of spikes (D). If such an orthogonal slice of the 3D reconstruction is oriented tangential to the surface of a virus, this also reveals the possibly hexagonal arrangement of the HEF trimers (H). The movie in the supporting information shows the succession of the slices through the cryo-ET 3D volume containing several virus particles with a dense population of spikes. It reveals that the hexagonal HEF clusters cover the surface of the particles, which is in line with the hypothesis that cluster formation drives virus budding.

For the mutant 653End, no major changes in the shape of the virus particles were obvious (Fig. 6), which is in contrast to Flu A with deleted cytoplasmic tails in HA and NA (43). In addition, most particles revealed internal densities that likely represent the viral genome. We counted the number of different particles across all tomograms for WT (*n* = 556) and 653End virions (*n* = 730). While 12.9% of WT viruses in the tomograms clearly showed a hexagonal arrangement of HEF trimers, only 6.8% of the mutant 653End revealed HEF clusters, and thus, the number of hexagonal HEF arrays was reduced by roughly 50%. Likewise, the number of particles with a dense population of spikes was also reduced from 18.5% (WT) to 4.8%, whereas the fraction of particles with a sparse population of spikes was increased from 64.7% (WT) to 84.4% in 653End. The number of particles without spikes remained the same (3.8%) in WT and 653End.

We also analyzed clustering of the HEF 653End mutant by dSTORM in the apical membrane of transfected MDCK I cells (Fig. 2E). Voronoi tessellation analysis (36) revealed that the fraction of HEF molecules organized in clusters was statistically significant reduced from 55% for WT HEF to 42%. We conclude that removal of the cytoplasmic tail of HEF compromises HEF clustering.

### Exchange of amino acids potentially involved in HEF hexamer formation

*Amino acids involved in interactions between trimers in the closed HEF conformation*

Having shown that expression of HEF alone is sufficient for formation of the hexagonal HEF clusters, we anticipated that

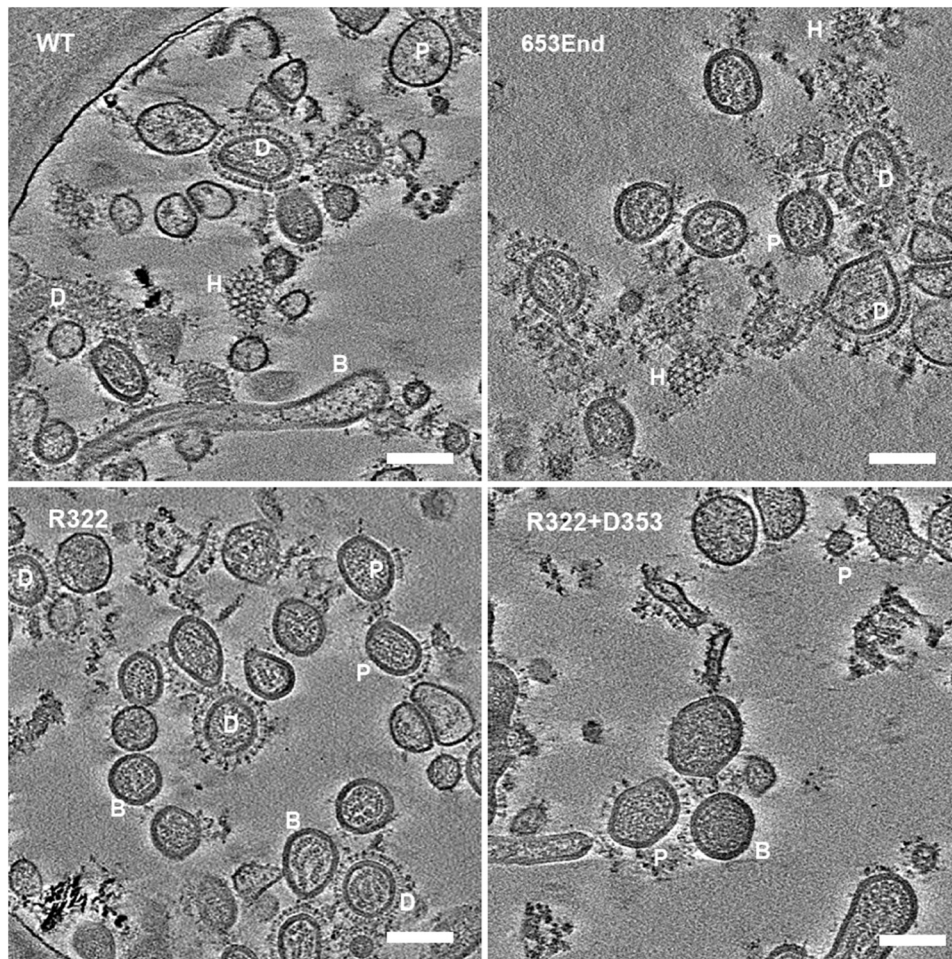


**Figure 6. Cryo-electron tomograms of Flu C virus particles purified from infected MDCK I cells.** WT Flu C and the indicated mutants were purified from cellular supernatants through a sucrose cushion. Sections of cryo-TEM micrographs illustrating the varying morphology of virus particles. B: bald particles completely lacking surface spikes. P: particles partly and D: particles densely covered with spikes. H: hexagonal arrangements of the HEF trimers are visible if orthogonal slice of the 3D reconstruction is oriented tangential to the surface of a virus. The scale bar corresponds to 100 nm. Flu C, influenza C; MDCK I, Madin-Darby canine kidney cells, subline I.

intertrimer interactions between amino acids are responsible for cluster formation. We therefore searched the head domain of the open HEF structure for amino acids with large side chains that are exposed at the periphery in the wider distal trimer region. We found that Arg 68, Lys 320, Arg 322, Glu 350, Asp 353, Gln 358, and Glu 362 might be able to interact with complementary residues in another HEF trimer (Fig. 7, A and B). Since HEF of Flu D also forms hexagonal arrays possibly by similar interactions (10), we superimposed both structures to identify conserved residues (Fig. 7B). The analysis revealed one positively charged amino acid, Arg (R) 322 (position 325 in Flu D), and two negatively charged residues, Glu (E) 350 (354) and Asp (D) 353 (357), as potential candidates that might form electrostatic interactions between trimers. The residues were exchanged to alanine, either alone or combinations where an acidic and a basic residue were exchanged simultaneously to analyze their effect on virus rescue and replication.

We could generate infectious virus particles for all single mutants and for the double mutant R322 + D353 but not (in

three attempts) for R322 + E350. Assessing the growth kinetics of the rescued viruses revealed that exchange of the basic residue R322 alone caused a significant drop in infectious virus titers by two logs (which is equivalent to a reduction by 99%) and also in HA titers, and the same reduction was seen if R322 and D353 were exchanged together. Likewise, the specific infectivity (PFU/HA ratio) of R322 and R322 + D353 was also reduced at all time points. In contrast, no differences to WT virus were observed for the mutants E350 and D353 (Fig. 8).

We then prepared virus particles of these two mutants, showing lower titers in cell culture, for microscopic analysis. Figure 6 (lower panels) shows sections of typical slices of cryo-ET-3Ds of the R322 and R322 + D353 mutants. Counting the number of different particles in the reconstructed tomography slices revealed that particles with hexagonal HEF array are greatly reduced in the mutants: While for R322, the hexagonal HEF array could only be detected in 2.8% of the viruses ( $n = 669$ ), for the double mutant, it was only 0.4% ( $n = 227$ ), compared to 12.9% for the WT ( $n = 556$ ). In general,

## Influenza C virus budding

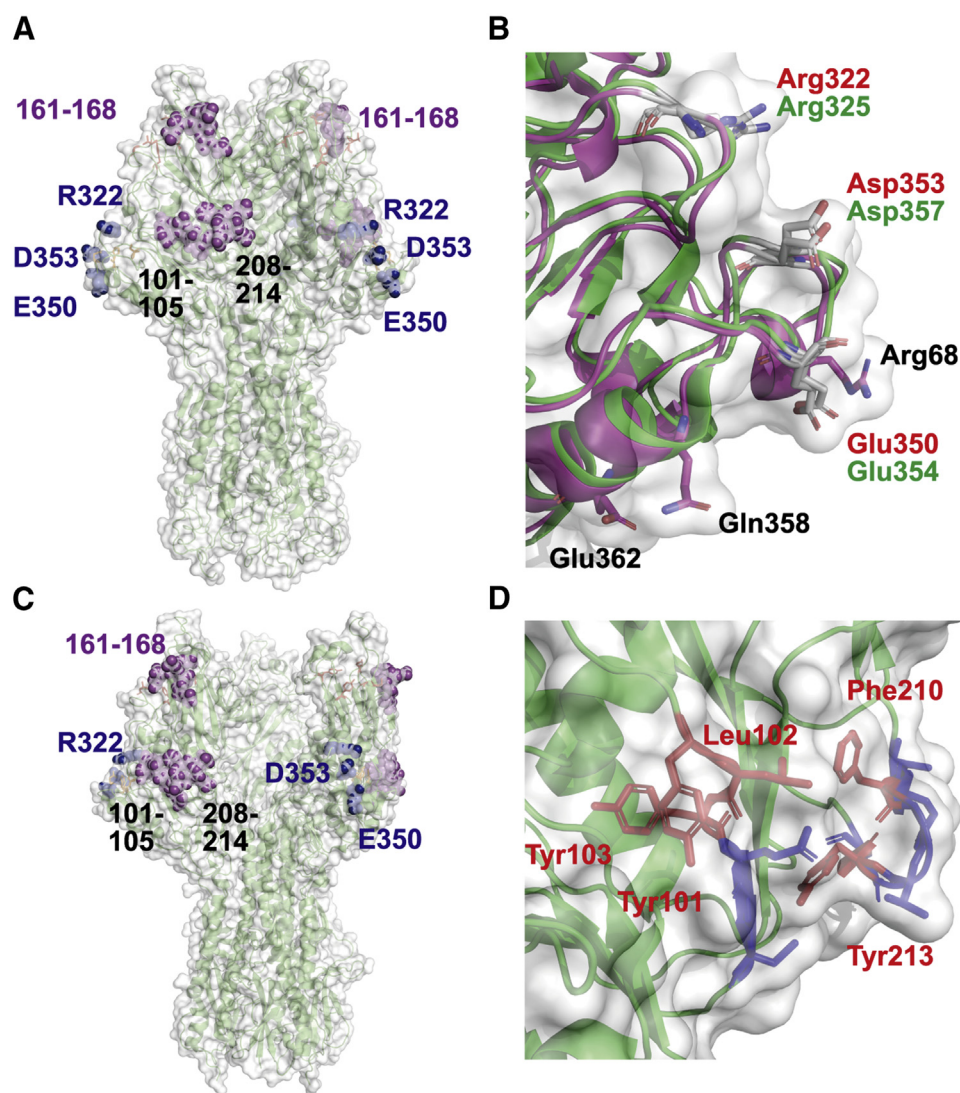


**Figure 7. Structure of HEF in the closed and open conformation.** *A*, surface representation of the ectodomain of a HEF trimer in the closed conformation. Amino acids supposed to contact other HEF trimers in the closed conformation are shown as *blue spheres* and in the open conformation as *purple spheres*. *B*, superpositioning of the structure of HEF from Flu C (*purple*) and Flu D (*green*) at the proposed contact region between trimers. Amino acids that might form contacts between Flu C HEF trimers are shown as *sticks*. Only residues conserved in HEF of Flu D are also shown as *sticks*. The surface corresponds to the surface of HEF from Flu C. *C*, surface representation of the ectodomain of a HEF trimer in the open conformation. Amino acids supposed to contact other HEF trimers in the closed conformation are shown as *blue spheres* and in the open conformation as *purple spheres*. *D*, detail of the structure of HEF in the open conformation. Amino acids 101 to 105 and 208 to 214, that are supposed to contact other HEF trimers (15), are shown as *sticks*. Amino acids exchanged to serine are shown as *red sticks* and labeled. Figures were created with PyMol version 2.1.1 using the following pdb-files: Flu C HEF in the closed conformation: 1FLC, Flu C HEF in the open conformation: 6YI5, and Flu D HEF in the closed conformation: 5E5W. Flu C, influenza C virus; Flu D, influenza D virus; HEF, hemagglutinin-esterase-fusion glycoprotein.

incorporation of the HEF spike into particles was apparently disturbed. Both mutants showed about 50% less number of particles with a dense population of spikes (9.3% [R322] and 8.7% [R322 + D353] *versus* 18.5% in WT) and a small reduction in the number of particles with a sparse population of spikes (77.8% [R322] and 80.7% [R322 + D353] *versus* 84.4% in WT), whereas the number of bald particles lacking spikes was increased around threefold (10.1% for both mutants *versus* 3.8% in WT).

In summary, we propose that Arg 322 interacts electrostatically with Glu 350 localized on an adjacent trimer. If Glu 350 is exchanged, Arg 322 might be able to interact with Asp 353. Exchange of Arg 322 might be partially replaced by other interactions not analyzed here, but in both cases virus

replication, HEF incorporation into virus particles and the formation of HEF clusters is substantially impaired.

### *Amino acids involved in interaction between trimers in their open conformation*

During the course of this study, the *in-situ* cryo-EM structure of HEF in intact virus particles was published (15), which revealed a large difference to the X-ray structure of the isolated ectodomain (13). The HEF1 head region is rotated 20° clockwise thereby generating a more open conformation. This movement creates other HEF1–HEF1 dimeric contacts between trimers that might also be an (additional) structural basis for the hexagonal surface lattice ((15), see Fig. 7, C and D).

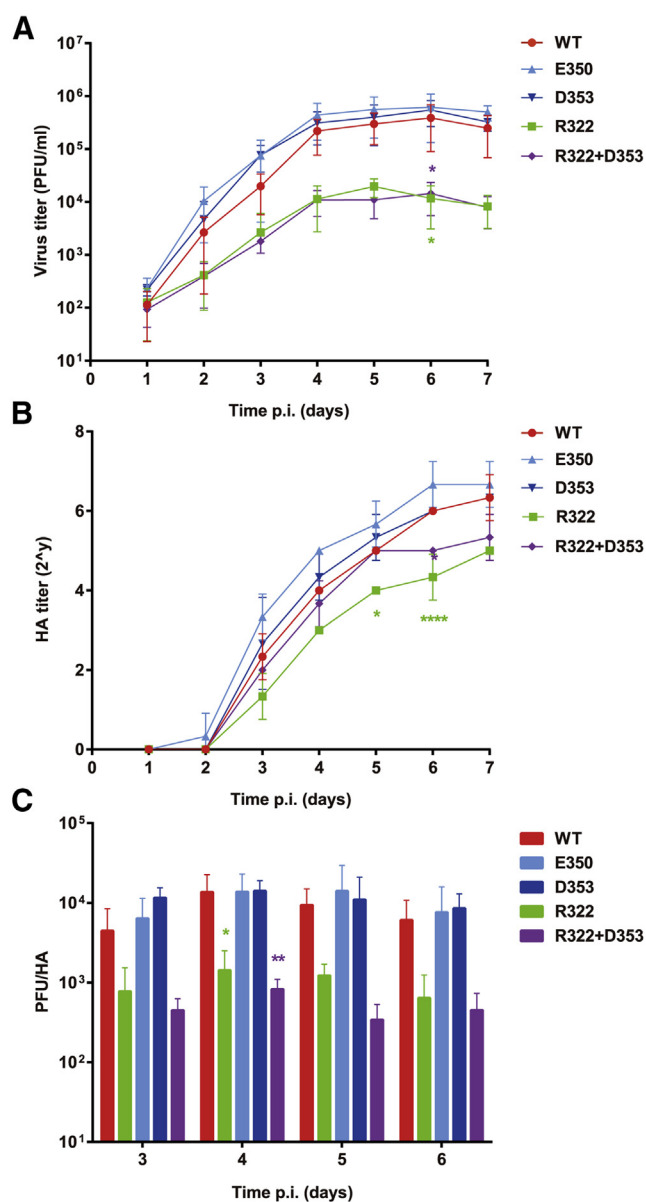


**Figure 8. Growth kinetics of Flu C WT and viruses with mutations in putative contact amino acids.** MDCK I cells in 24-well plates were infected at an MOI of 0.05 with Flu C, WT or mutants where the indicated amino acids were exchanged by a serine. *A* and *B*, culture supernatants were collected at the indicated time points, and titers were determined with a fluorescence-based plaque assay (*A*) or an HA assay (*B*). *C*, ratio of PFU to HA titers were calculated for the indicated time points. The graph shows the mean titers with standard deviations (error bars) from three independent infections. The asterisks indicate statistically significant differences ( $*p < 0.05$ ,  $**p < 0.01$ ,  $***p < 0.001$ ,  $****p < 0.0001$ ) between WT and the mutants. One-way ANOVA followed by Tukey's multiple comparison test was applied for statistical analysis. Flu C, influenza C virus; HA, hemagglutinin; HEF, hemagglutinin-esterase-fusion glycoprotein; MDCK I, Madin-Darby canine kidney cells, subline I.

Three regions were identified that might either form homotypic contacts (loop 161–168 located near the receptor-binding site, amino acids TIPLQATAG) or heterotypic contacts between trimers, region 101 to 106 (**YLYQGC**) with loop 208 to 214 (**TQFGTYE**). After searching for residues that are conserved in HEF of Flu D (highlighted in *bold*), we selected several residues in region 101 to 106 and loop 208 to 214

(underlined) for mutagenesis. We assumed that Tyr 101, Leu 102, and Tyr 103 form hydrophobic interactions with Phe 210 and Tyr 213, and therefore, we exchanged these residues by serine, either in one region (mutant Y101S + L102S + Y103S, named 3S and mutant F210S + Y213S, named 2S) or in both regions together (mutant Y101S + L102S + Y103S + F210S + Y213S, named 5S). However, in three independent attempts, we were not able to generate infectious virus particles for any of the mutants, although WT virus could be rescued in parallel and yielded HA titers of  $2^7$  or  $2^8$  after one amplification in MDCK I cells. Furthermore, supernatants from MDCK I cells were also used to infect fresh cell, but 2 days later, no HEF-positive cells were detected by immunofluorescence (not shown). We conclude that the amino acids suggested to form lateral interactions between HEF trimers are essential for virus replication.

#### Intracellular transport and processing of HEF mutants

Since we could not analyze the role of putative HEF contact residues in the context of virus replication, we asked whether these HEF mutants are able to create protein particles if expressed from a plasmid. Since HEF is known to be temperature sensitive, *i.e.*, proper folding is favored at  $33\text{ }^\circ\text{C}$  compared to  $37\text{ }^\circ\text{C}$  (44), all subsequent experiments were performed at the lower temperature. Western blotting of lysates from transfected HEK-293T cells revealed large differences in band intensities between WT HEF and the mutants (Fig. 9A). Especially the mutations that we hypothesize to destroy contacts between trimers reduced HEF expression strongly. In contrast, HEF mutants lacking the cytoplasmic tail are expressed at similar levels as WT HEF. Some of the poorly expressed HEF mutants also exhibit a slightly different band pattern (*e.g.*, R322 + E350, 5S), suggesting differences in carbohydrate processing due to a blockade of their intracellular transport. We therefore quantified the number of WT and mutant HEF proteins at the surface of transfected HEK-293T cells using antibody staining and flow cytometry. One aliquot of cells was permeabilized to determine total HEF expression levels; the other was left untreated to estimate cell surface-localized HEF. The mean fluorescence intensity from  $10^4$  cells (minus background fluorescence of untransfected cells) was determined. Ratios of surface *versus* total expression were calculated, and results were normalized against WT HEF (=100%). The resulting graph (Fig. 9B) from three different transfections revealed that surface expression of the mutants 2S, 3S, 5S, and R322 + E350, which could not be rescued from plasmids, is greatly reduced to 40%, 5%, 10%, and 20%, respectively. Other mutations (R322, R322 + D353) that we hypothesize to affect HEF clustering and which exhibit reduced growth rates in cell culture also exhibit surface exposure reduced by approximately 40%. In contrast, HEF oligomerization mutants that revealed no reduced growth in cell culture (E350, D353) and mutants lacking the cytoplasmic tail are exposed at the plasma membrane to a similar extent as WT HEF.

To investigate in which intracellular compartment the transport of the mutants is arrested, we performed

## Influenza C virus budding

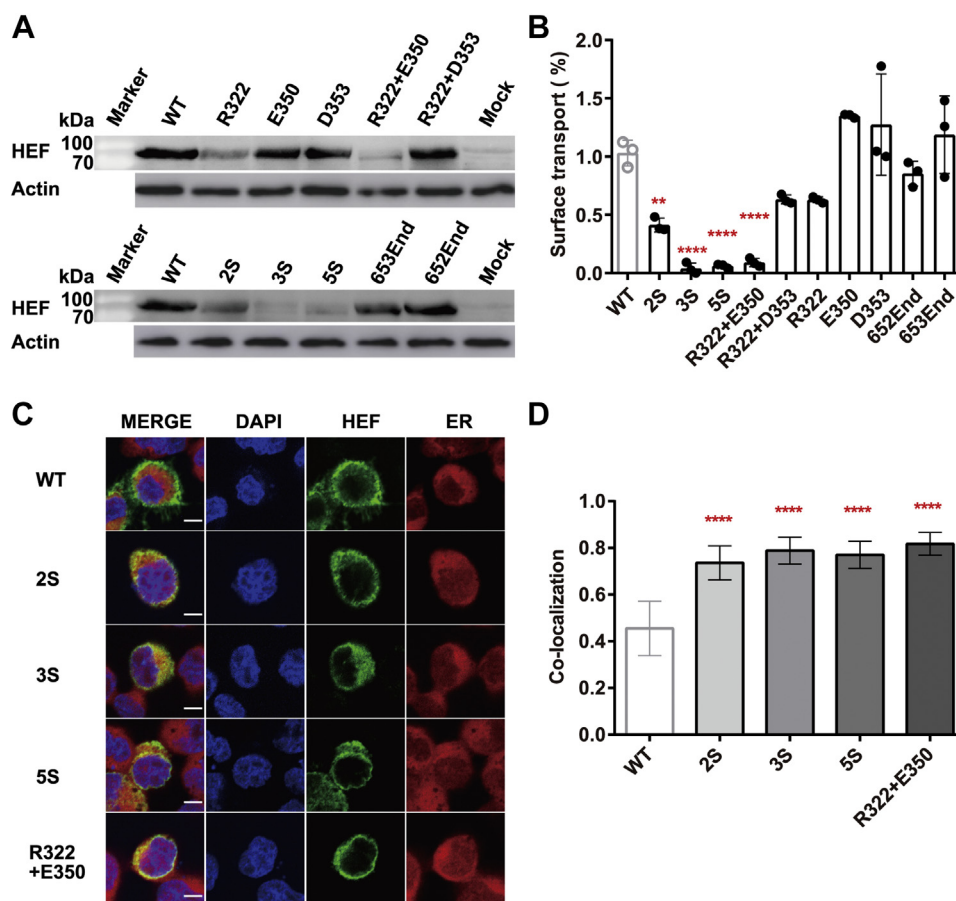


**Figure 9. HEF with mutations in putative contact amino acids is retarded in intracellular transport.** A, HEK-293T cells expressing the indicated HEF proteins were lysed after transfection, and an aliquot was subjected to SDS-PAGE and Western blotting with anti-HEF antiserum and anti-actin antibodies as loading control. B, quantification of surface exposure of HEF mutants by flow cytometry. HEK-293T cells were fixed at 48 h after transfection and either directly stained with anti-HEF antiserum (surface expression) or permeabilized prior to staining (total expression). The mean fluorescence intensity (MFI) from at least 10,000 cells of three different transfections was determined by flow cytometry. The results were normalized against the surface expression of WT HEF for each transfection, and the relative surface expression is plotted against the total expression for each protein. The asterisks indicate statistically significant differences ( $*p < 0.05$ ,  $**p < 0.01$ ,  $***p < 0.001$ ,  $****p < 0.0001$ ) between WT and the mutants. One-way ANOVA followed by Tukey's multiple comparison test was applied for statistical analysis of three independent experiments. C, localization of HEF in transfected cells. CHO-K1 cells were transfected with WT (upper panel), or with F210Y213 (2S, second from above), or with Y101L102Y103 (3S, third panel), or with F210Y213 + Y101L102Y103 (5S, fourth panel) and R322 + E350 (lower panel). HEF was stained with polyclonal anti-serum against the HEF followed by secondary anti-rabbit antibodies coupled to Alexa Fluor-488 fluor, ER with ER staining Kit-Red Fluorescence-Cytopainter from Abcam and nuclei with DAPI. Scale bar: 5  $\mu$ m. D, colocalization of HEF with ER from at least 40 cells from three different transfections was quantified with the Pearson's correlation coefficient method using the JACoP plugin of the ImageJ software. The asterisks indicate statistically significant differences ( $*p < 0.05$ ,  $**p < 0.01$ ,  $***p < 0.001$ ,  $****p < 0.0001$ ) between WT and the mutants. One-way ANOVA followed by Tukey's multiple comparison test was applied for statistical analysis. CHO-K1, Chinese hamster ovary cells; ER, endoplasmic reticulum; HEF, hemagglutinin-esterase-fusion glycoprotein; HEK-293T, human embryonic kidney-293T cells.

colocalization experiments with an ER marker for the HEF mutants having the lowest cell surface exposure. Whereas the Pearson's correlation coefficient for colocalization of WT HEF with the ER marker is around 0.4, the value is doubled to 0.8 for the mutants 2S, 3S, 5S, and R322 + E350. We conclude that these HEF mutants are retained in the ER, probably because cluster formation is a prerequisite for intracellular transport.

## Discussion

### Role of CM2 for virus assembly and budding

CM2 is transported to the plasma membrane if expressed alone and causes release of particulate antigen into the cellular supernatant which appeared in negative-stain EM as long filaments (Figs. 1, 3, and 4). This indicates that CM2 has the ability to tubulate membranes. If CM2 is co-expressed with

CM1 and especially with HEF, the particles exhibit a more virus-like appearance in EM, but less CM2 was detected in the supernatant as evidenced by Western blotting (Fig. 3). This suggests that CM2 might be displaced by the viral glycoprotein from the budding site. Accordingly, CM2 is expressed in large numbers at the surface of virus-infected cells, but only a small amount is incorporated into virus particles (45).

M2 of Flu A has very similar properties. It is abundantly expressed at the plasma membrane, but only poorly incorporated into virus particles (46). It can be released into the supernatant of transfected cells, but the morphology of these particles was not investigated (28). The purified protein is able to bud into GUVs, which is mediated by an amphiphilic helix located adjacent to the transmembrane region (47). In the context of virus replication, the helix is supposed to insert into the inner membrane leaflet at the budding site to induce

curvature that causes virus scission (28). Structural data are not available for CM2, but a heliquet analysis (<https://heliquet.ipmc.cnrs.fr/cgi-bin/ComputParams.py>) using the 18 amino acids adjacent to the transmembrane region predicts an amphiphilic helix with charged amino acids in its hydrophilic face (Fig. S1). In addition, two biophysical properties of the helix, overall hydrophobicity and the hydrophobic moment, are almost identical in M2 and CM2, although both peptides exhibit no amino acid homology. However, there is considerable sequence variation in the helix among Flu A strains, and the helix tolerates a large number of amino acid exchanges and can be replaced by helices from cellular proteins without a strong effect on its functionality as long as the hydrophobic moment of the helix is preserved (48–50). It is thus tempting to speculate that the membrane-near region of CM2 forms an amphiphilic helix, which is involved in membrane tubulation and performs a similar function during the viral replication cycle, e.g., scission and release of virus particles. Likewise, heliquet predicts that the membrane-near region of the M2 protein of Flu D also forms an amphiphilic helix. In contrast, the cytoplasmic domain of BM2 of Flu B is a helical extension of the transmembrane region, which does not run perpendicular to the membrane and hence is unlikely to exert a pushing force on the bilayer (51)

### Role of CM1 for virus assembly and budding

CM1 was not detected in the nucleus of transfected cells (Fig. 1), which is a remarkable difference to the matrix proteins of Flu A and Flu B especially if considering the pivotal role of M1 for nuclear export of the viral genome (52). However, other have reported that CM1 antigen was detected in the nucleus of cells infected with the Flu C strains C/Yamagata/1/88 and C/Ann Arbor/1/50, albeit CM1 of the latter strain only weakly (53). The amino acid sequence of CM1 from C/Yamagata/1/88 and C/Ann Arbor/1/50 are identical but differ in one position (residue 182 is Met in Ann Arbor and Yamagata, but Ile in JJ) from CM1 of C/JJ/1/50, which seems unlikely to prevent nuclear transport. We rather assume that differences between transfected and virus-infected cells contribute to differences in CM1 targeting. However, note that the signals required for shuttling of proteins between the cytosol and the nucleus, a basic nuclear localization sequence and a nuclear export signal that have been identified for M1 of Flu A and Flu B (35, 54, 55), are not present in CM1.

Upon expression from its plasmid, CM1 is targeted *via* the Golgi apparatus to the plasma membrane where it caused release of ellipsoid and spherical vesicles of various sizes into the supernatant indicating that CM1 is able to vesiculate membranes (Figs. 1, 3, and 4). This is consistent with the observation that purified CM1 binds to GUVs *in vitro* where it induces inward budding of membrane tubules with diameters that resemble the diameter of viruses (31). Likewise, CM1 is responsible for the formation of long surface protrusions in cells infected with certain Flu C variants. These cord-like structures consist of numerous filamentous particles in the

process of budding, which are aggregated with their long axes (56, 57).

For Flu A, it was initially proposed that M1 is the driving force for virus budding (58), but a subsequent study suggested that VLP release was likely due to overexpression of the protein with a vaccinia virus system (38). However, M1 is not transported to the plasma membrane in transfected cells but localizes, besides the nucleus and the cytosol, to the ER and mainly to the Golgi region (20, 34). It was thus proposed that the failure to be transported to the plasma membrane is the reason for its inability to release VLPs. Indeed, if M1 is equipped with an N-terminal acylation signal, it is transported to the cell surface and is able to release protein particles (20). Likewise, co-expression with M2 recruits M1 to the plasma membrane and causes particle release (23). Upon binding to the plasma membrane, M1 oligomerizes which provides a pushing force that bends the membrane (59, 60). Similar detailed studies have not been performed with CM1 yet, but purified CM1 folds into an elongated structure that associates laterally into ring-like or filamentous polymers (31). The vesicles we observed were partially or completely filled with electron-dense material which likely represent these CM1 oligomers.

Thus, we conclude that M1 and CM1 probably play a very similar role in virus budding. Both proteins associate with the Golgi complex, but only CM1 is intrinsically targeted to the plasma membrane. The differences in trafficking might be due to subtle differences how both proteins associate with membranes.

Membrane binding of M1 of Flu A is mediated by interactions between negatively charged phospholipids, such as phosphatidylserine, which are enriched at the inner leaflet of membranes with basic residues in the N-terminal domain of M1, Arg76, Arg 77, and Arg 78 in helix 5, Arg 101 and Lys 104 in helix 6, and Arg 134 in helix 8 (34, 61, 62). In addition, computational simulations identified an interaction of Gln75/Gln81 with phosphatidylcholine (63). CM1 also needs negatively charged lipids to bind to GUVs suggesting that membrane binding is mediated by similar means (31). Superpositioning of the crystallized N-terminal domains of the M1 structures of Flu A and Flu C revealed that their overall folding is very similar (31) (Fig. S2A), despite a low amino acid identity of 17.7% and similarity of 36.0%.

Not all of the residues mediating contact to lipids in M1 are conserved in CM1 or are not exposed at the molecule's surface. However, assuming that CM1 associates with the same surface as M1 to membranes, CM1 of Flu C also contains surface exposed basic residues, Lys 41 and Lys 44 in helix 3, Lys 70, 73, and 81 in helix 5, Lys87, Lys 88, Arg 92, and Lys 96 in helix 6 (Fig. S2B). In addition, CM1 contains two Mg<sup>2+</sup> ions coordinated by residues from helices 5 and 8, which might increase the positive charge of the surface near the prosed membrane binding domain (31). Thus, although M1 and CM1 both associate *via* electrostatic interactions with membrane, subtle differences in the binding mode might be decisive for retention in the Golgi or subsequent transport to the plasma membrane.

## Influenza C virus budding

Since structures of M1 of Flu B and Flu D are not available, we used the artificial intelligence program alphafold2 (64), which is freely available on the Internet *via* a Google colab notebook (<https://colab.research.google.com/github/sokrypton/ColabFold/blob/main/AlphaFold2.ipynb>) to predict the structures of their N-terminal domains. The reliability of both predictions is very high, demonstrated by the Local Distance Difference Test (pIDDT) scores of up to 95 (out of 100, not shown). Especially, the  $\alpha$ -helical elements are predicted with high precision, as indicated by the color coding (from red to blue) of the predicted structure (Figs. S3A and S4A). Red (corresponding to pIDDT scores of 90 and higher) indicates very high accuracy, equivalent to structures determined by experiments, which allows to investigate details of individual side chains. Superpositioning of the predicted structures with the experimentally determined structures of M1 of Flu A and Flu C, respectively, revealed that they are almost identical (Figs. S3B and S4B). Moreover, the basic residues involved in membrane binding are located at the same or very similar positions (Figs. S3C and S4C). Thus, it is very likely that M1 proteins of all influenza virus genera associate *via* basic amino acids with the lipid bilayer, and this interaction might allow them to execute a pushing force on the membrane.

### Role of HEF for virus assembly and budding

HEF is also transported to the plasma membrane when expressed from a plasmid (Fig. 1). Super resolution microscopy revealed HEF clusters with an average diameter of about 250 nm in the apical membrane of fixed MDCK I cells, which corresponds to the expected size of virus buds (Fig. 2). Furthermore, expression of HEF caused release of membranous vesicles exhibiting the typical hexagonal arrays (Fig. 3). In contrast to HA of Flu A (23, 38), vesicle release is not dependent on addition of exogenous neuraminidase activity, since HEF possess its own receptor-destroying esterase activity which can release the protein from the cell surface. The HEF clusters are concentrated in some areas of the vesicle, where they form structures resembling various stages of virus budding (Fig. 4). Furthermore, the HEF clusters cover the whole surface of WT particles and hence form an external coat which could sculpt a vesicle out of the planar plasma membrane (Movie S1). This observation confirms and extends previous findings that formation of the hexagonal arrangement is an intrinsic feature of HEF and does not require other viral proteins (11, 12). Furthermore, these experiments provide evidence that formation of the regular HEF arrays is one driving force for virus budding.

We then investigated which molecular mechanism might cause clustering of HEF. One possibility is its association with cholesterol-enriched nanodomains which enrich the viral protein at the viral assembly site, as shown for HA of Flu A. These HA assemblies are often stabilized by elements of the cytoskeleton, especially cortical actin filaments (21, 22). However, the HEF clusters observed by super resolution microscopy are insensitive to cholesterol extraction and also to

cytochalasin treatment, the latter prevents polymerization of actin (Fig. 2). The cholesterol-independent clustering of HEF is consistent with the observation that HEF, in contrast to HA, does not associate with detergent-resistant membranes (65). Therefore, we propose that HEF does not need to be concentrated by extrinsic elements, such as association with membrane domains or the cytoskeleton, since it has an intrinsic self-assembly functionality based on lateral interactions between trimers.

Although the hexagonal HEF arrays form in the absence of other viral proteins, it has been suggested that interactions of CM1 with HEF stabilizes the clusters (15). Deletion of the short cytoplasmic tail Arg-Thr-Lys (mutant 653End) delayed replication of recombinant virus and reduced virus titers by one log. When the adjacent acylation site was also removed (mutant 652End), this effect was much more pronounced (Fig. 5). Due to the greatly reduced number of released particles, we could not purify the latter virus, but the mutant 653End revealed a slight reduction of HEF arrays in cryo-ET, and the overall shape of virus particles was not disturbed (Fig. 6).

Both cytoplasmic tail mutants revealed no reduced expression levels in transfected cells and are transported to the plasma membrane, which is in contrast to the mutants that are supposed to mediate lateral interactions between the ectodomain of HEF (Fig. 9). These results are consistent with the concept that interactions between HEF and CM1 stabilize the HEF clusters. Note that the large reduction in virus titers in mutant 652End might be also due to other functional HEF defects, such as membrane fusion. If only the acylation site at position 652 of HEF is exchanged, a small impairment of its membrane fusion was observed (42), and this effect might be more pronounced if the whole cytoplasmic tail is deleted.

The effect on virus replication and HEF cluster formation was stronger if charged amino acids located at the surface of the molecule near its widest region in the closed HEF conformation were exchanged. Exchange of the pair Arg 322 plus Glu 350 by alanine prevented virus rescue, and exchange of the pair Arg 322 plus Asp 353 and also of Arg 322 alone reduced virus titers by 99% (Fig. 8) and also the number of hexagonal HEF arrays in virions (Fig. 6). We propose that Arg 322 in one trimer forms an ionic interaction with Glu 350 in another trimer which initiates HEF clustering. If Glu 350 is exchanged, Arg 322 might be able to interact with Asp 353, and the loss of Arg 322 might be compensated by other interactions, but in both cases, virus replication and HEF clusters are impaired.

The effect on virus viability was even stronger if amino acids were exchanged that were proposed to form interactions between trimers in the *in-situ* structure of HEF (15). Exchange of two hydrophobic amino acids in region 101 to 106, three in loop 208 to 214, and all five amino acids together by serine abrogated rescue of infectious virus particles. All mutations proposed to impair interactions between HEF trimers revealed common processing defects in transfected cells. Their expression levels were greatly reduced relative to WT HEF, and their transport to the plasma membrane was inefficient;

most of the molecules remained in the ER (Fig. 9). Of course, this precludes further analysis, so we can only speculate about the molecular mechanism causing these defects.

The relationship between the closed structure of HEF determined from its ectodomain and the open *in-situ* structure is unclear. Obviously, however, the latter form represents the native HEF structure in virus particles, and it was proposed that it already had performed the first of the conformational changes that cause membrane fusion (15). Hence, we assume that the closed HEF structure might be a transient precursor that exists only inside cells. We propose that during protein synthesis in the ER, HEF first folds into the closed structure. Lateral interactions of Arg 322 with mainly Glu 350 cause clustering of HEF trimers. HEF is then converted into the open conformation which associates *via* hydrophobic interactions between amino acids in region 101 to 106 with amino acids in loop 208 to 214 and possibly by homotypic contacts between residues in loop 161 to 168 not investigated here. We further speculate that clustering of HEF is a requirement for efficient transport of the protein to the plasma membrane. In general, only properly folded proteins can exit the ER, and unfolded proteins are removed by the quality control system and degraded in the proteasome (66). Such a mechanism would explain the lower expression levels of the HEF mutants, which we think are unlikely to be due to decreased protein synthesis. We speculate further that exchange of amino acids located in loops at the surface of the trimer is unlikely to affect initial folding of monomeric HEF once it is translocated into the lumen of the ER. We rather assume that they subsequently affect clustering of trimers, which seems to be a prerequisite for its intracellular transport. Why only presumably rather small HEF clusters are efficiently transported remains open and requires further investigation.

It is also unknown what cues cause the conformational change of HEF from the closed to the open structure and how the latter stabilizes clusters. Comparing both structures revealed subtle differences in the putative contact region of the closed conformation (Fig. S5). The side chain of Lys 320 is rotated by around 120° in the open structure which allows its -NH<sub>3</sub> group to interact with the carboxyl group of Asp 353 that neutralizes its negative charge. Since Asp 353 might interact with Arg 322, the rotation of Lys 320 might destabilize this interaction and allows the HEF trimers to switch to the open conformation. Small molecules could be designed that block the proposed interaction and hence would likely inactivate the HEF spike. Electrostatic interactions might also be involved in the formation of NA clusters observed on the surface of Flu A virus particles. It has been speculated that these NA-clusters might contribute to virus budding and hence blocking their interaction might reduce virus replication (21).

In summary, our study on assembly and budding of Flu C revealed common but also distinct features compared to Flu A. Most surprisingly, CM1 was not detected in the nucleus of transfected cells indicating that nuclear export of the viral genome occurs by a mechanism different from that established for Flu A and Flu B. CM1 was transported to the plasma

membrane in the absence of other viral proteins, whereas M1 is retained in the Golgi. CM1, like M1 if localized to the plasma membrane can release membranous vesicles into the supernatant of transfected cells indicating that it can bend and vesiculate membranes. CM2, like M2, can also tubulate membranes, probably using an amphiphilic helix adjacent to the transmembrane region. A new principle may be realized in budding of Flu C viruses, namely the formation of an extrinsic coat by lateral interactions between the ectodomains of the glycoprotein HEF. In some other virus families, for example flaviviruses, budding is also primarily driven by interactions between membrane glycoproteins. However, they form a flat, symmetric, icosahedral lattice that drives viral morphogenesis by interactions mainly between transmembrane helices (25). In contrast, Flu C viruses are pleomorphic, and the only spike protein HEF does not lie flat on the membrane but forms long surface projections. Flu A do not show a regular network of its glycoproteins HA and NA, but lateral interactions might be involved in the smaller clusters of neuraminidase NA observed at the ends of filamentous virions or VLPs (23, 67).

## Experimental procedures

### Cell culture

HEK-293T cells, MDCK I, CHO-K1, and Vero cells were maintained in Dulbecco's modified Eagle medium (DMEM; Pan Biotech) supplemented with 10% fetal calf serum (FCS) and penicillin–streptomycin (100 µg/ml) at 37 °C and 5% CO<sub>2</sub>.

### Mutagenesis and generation of recombinant Flu C

To express HEF, CM1, and CM2 from Flu C (C/JJ/50), their genes were cloned from the pPMV plasmids used for reverse genetics (68) into the expression plasmid pCAGGS. The HEF coding sequence was amplified by PCR and subcloned using the restriction endonuclease *XhoI*. The CM1 and CM2 coding sequence were subcloned into the same plasmid using restriction endonucleases *XhoI* and *BglII*. CM2 was cloned without the N-terminal signal peptide, and a start codon was inserted with the primer. Both were equipped with a C-terminal tag, either 6xHis tag (CM1) or an HA-tag (CM2) using the appropriate primer. Mutagenesis was performed in the pPMV plasmids using the two-step overlap extension PCR method as described (42). To prevent reversion to WT virus, the amino acid exchanges described in the text were performed by exchanging at least two nucleotides. An exception is the HEF mutants lacking the cytoplasmic tail where the codon Cys652 (TGG) and Arg653 (AGA) were replaced by the stop codon TGA. Correctness of the mutations was confirmed by sequencing of the respective plasmid (LGC Genomics).

Rescue of infectious virus particles was performed as previously described (42). Ninety percent confluent Vero cells seeded on 6-well cell culture plates (Sarstedt) were transfected with seven bidirectional plasmids (4 µg total) and 10 µl Lipofectamine 2000 (Invitrogen) according to the manufacturer's instruction. Six hours posttransfection, cells were washed three times with phosphate-buffered saline (PBS) and incubated in

## Influenza C virus budding

3 ml serum-free Opti-MEM medium (Invitrogen) supplemented with a final concentration of 2 µg/ml TPCK-trypsin at 33 °C. Three or 4 days after transfection, supernatants were harvested, supplemented with 2 µg/ml TPCK-trypsin and used for infection of MDCK I cells grown in 6-well plates. Additional TPCK-trypsin (2 µg/ml) was added to the medium every second day. At 6 to 7 days postinfection, culture supernatants were harvested, centrifuged at 5000g for 10 min to clear it from cell debris. HA assays were performed, which usually resulted in a titer of 2<sup>7</sup> for WT virus. Samples that did not exhibit an HA titer were also used to infect MDCK I cells and tested 2 days later for HEF synthesis by immunofluorescence, which was also negative.

The resulting virus stock was titrated and stored at -80 °C. To determine the correctness of mutant viruses, viral RNA was extracted using innuPREP Virus TS RNA Kit (Analytik Jena AG), and the HEF gene was reverse transcribed with QIA-GENOneStep RT PCR Kit (Qiagen) according to the manufacturer's protocol. PCR products of the HEF gene were purified from agarose gels using the Monarch PCR & DNA CleanUp Kit (NEB) and sequenced (LGC Genomics).

### Determination of viral growth kinetics and virus titration

To determine the viral growth kinetics, 90% confluent MDCK I cell in 24-well plate were infected with WT or mutant Flu C at a MOI of 0.05 for 1 h. The inoculum was then replaced by fresh DMEM medium containing 2 µg/ml TPCK-trypsin and 0.1% fetal bovine serum, and cells were incubated at 33 °C. Aliquots of cell supernatants were collected at 24, 48, 72, 96, 120, 144, and 168 h postinfection. Viral titers were determined by TCID<sub>50</sub> (Fig. 5) or a fluorescence-based plaque assay (Fig. 8) as well as with HA assay.

**TCID<sub>50</sub>:** viruses were serially 10-fold diluted with DMEM medium containing 2 µg/ml TPCK-trypsin, followed by inoculating 100 µl onto confluent MDCK I cells grown on a 96-well plate. Every second day, 20 µl fresh DMEM medium with TPCK-trypsin (10 µg/ml) was added to keep the final concentration of TPCK-trypsin at 2 µg/ml. At 6 days postinfection, 96-well plates were centrifuged at 1000 rpm for 10 min, and supernatants were harvested. The highest dilution of the supernatant, which was able to hemagglutinate chicken erythrocytes, was considered as the endpoint, and the TCID<sub>50</sub> was calculated by the method of Reed and Muench, and it was converted into PFUs according to the formula  $PFU = 0.7 \times TCID_{50}$ .

**Fluorescent plaque assay:** viruses were serially 10-fold diluted with DMEM medium containing 2 µg/ml TPCK-trypsin, followed by inoculating 500 µl onto confluent MDCK I cells grown on a 6-well plate. After 1 h incubation at 37 °C with shaking every 15 min, cells were washed three times with PBS and overlaid with 1.2% Avicel (FMC BioPolymer), 1% NaHCO<sub>3</sub>, 0.1% FCS, 0.2% BSA, and 2 µg/ml TPCK-trypsin. After incubation for 5 days at 33 °C, media were removed, and cells were washed three times with PBS. Cells were then fixed with 4% (wt/vol) paraformaldehyde in PBS for 20 min, blocked (3% BSA in PBS for 1 h), and incubated with

polyclonal rabbit anti-HEF antiserum (1:1000 in PBS supplemented with 3% BSA,) for 1 h and then anti-rabbit secondary antibody coupled to Alexa Fluor 488 (1:1,000; Sigma) for 30 min. Cells were washed three times with PBS (each for 2 min) after each antibody incubation. Cells were inspected, and fluorescent plaques were counted with a Zeiss Axio Vert A1 inverse epifluorescence microscope.

HA assays were performed in 96-well V-bottom plates. Viruses were serially 2-fold diluted with 50 µl PBS and added to 50 µl 1% chicken red blood cells to every well. After incubation for 30 min at room temperature, HA titers were recorded.

### Analysis of released protein particles by SDS-PAGE and Western blotting

HEK-293T cells grown in 6-well plates were transfected with 2.5 µg of each plasmid using lipofectamine 2000 as described by the manufacturer. Forty-eight hours later, supernatants were harvested, cleared from cell debris (5000g for 30 min), and pelleted (28,000g for 2 h) through a 20% sucrose cushion. The pellets were dissolved in PBS, and 5× reducing SDS-PAGE sample buffer was added, and samples were heated for 10 min at 95 °C. Cells were also lysed in lysis buffer (0.5% NP-40, 500 mM Tris-HCl pH7.4, 20 mM EDTA, 30 mM sodium pyrophosphate decahydrate, 10 mM sodium fluoride, 1 mM NEM, and protease inhibitor), 5× reducing SDS-PAGE sample buffer was added, and samples were heated for 10 min at 95 °C. Cell lysates or pellets were subjected to 12% SDS-PAGE under reducing condition. Gels were blotted onto polyvinylidene difluoride membrane (GE Healthcare). After blocking of membranes (blocking solution: 5% skim milk powder in PBS with 0.1% Tween-20) for 1 h at room temperature, anti-HEF polyclonal antiserum (diluted 1:3000 in blocking solution), anti-6x-His tag antibody (PA1-9531, diluted 1:1000 in blocking solution, Invitrogen), and anti-HA tag antibody (ab9110, diluted 1:10,000 in blocking solution, Abcam) were applied overnight at 4 °C. After washing (3 × 10 min with PBS with 0.1% Tween-20), horseradish peroxidase-coupled secondary antibody (anti-rabbit or anti-chicken, 1:1000, Sigma-Aldrich) was applied for 1 h at room temperature. After washing, signals were detected by chemiluminescence using the ECL Plus reagent (Pierce/Thermo) and a Fusion SL camera system (Peqlab). The density of bands was analyzed with ImageJ software and quantified by Graph-Pad Prism.

### Confocal microscopy to analyze intracellular localization of viral proteins

CHO-K1 cells grown in 24-well plates were transfected with the corresponding plasmids. Twenty-four hours later, the cells were fixed with 4% paraformaldehyde for 20 min at room temperature, permeabilized with 0.1% Triton in PBS for 10 min at room temperature. After blocking (3% BSA in PBS) for 1 h at room temperature, cells were incubated with the following primary antibodies for 1 h at room temperature: rabbit-anti-HEF antiserum (1:1000), chicken anti-6x-His tag antibody (PA1-9531, Invitrogen, 1:1000), and mouse anti-HA

tag antibody (26183, Invitrogen, 1:1000). Then anti-rabbit (A11011, Invitrogen) secondary antibody coupled to Alexa Fluor 568, anti-chicken (A11039, Invitrogen) secondary antibody coupled to Alexa Fluor 488, and anti-mouse (A21235, Invitrogen) secondary antibody coupled to Alexa Fluor 647 were diluted 1: 10,000 and incubated for 1 h at room temperature. ER was stained with ER staining Kit Red Fluorescence-Cytopainter (ab139482, Abcam) for 30 min at room temperature. Golgi was stained with cis-Golgi marker GM130 rabbit monoclonal antibody (1:200) or Golgi marker 58K mouse monoclonal antibody (1:500) from Abcam. Nuclei were stained with DAPI. Washing with PBS (three times, each for 2 min) was performed between each step. Pictures were recorded using the Nikon inverted microscope Eclipse Ti (Visitron Systems GmbH). Colocalization of viral proteins with organelle markers was quantified with the Pearson's correlation coefficient method from at least 40 cells using the JACoP plugin of the ImageJ software.

### Super resolution fluorescence microscopy

For dSTORM imaging, MDCK I cells grown on 8-well glass bottom dishes (Sarstedt) were transfected with plasmid (1  $\mu$ g) using Turbofect or infected with Flu C (MOI = 1). Twenty-four hours later, samples were fixed with 10% PFA for 10 min, blocked with PBS (5% BSA) for 30 min and labeled in PBS (5% BSA) using mouse Ab IgG anti-HEF antibody (1:20,000, a generous gift by Prof. Dr J. Vlasak) followed by labeling with Alexa Fluor 647 goat Ab IgG anti-mouse IgG (1:1000, Invitrogen, A-21235). For extraction of cholesterol, cells were incubated with 5 mM methyl- $\beta$ -cyclodextrin in DMEM<sub>10</sub> (DMEM with 10% FCS (v/v), 1% Penicillin/Streptomycin (v/v), 2 mM L-glutamine) for 60 min. Actin polymerization was inhibited by incubation with 1  $\mu$ M cytochalasin A in DMEM<sub>10</sub> for 60 min.

Imaging was performed with a homebuilt wide-field microscope as described by others (69). TetraSpeck Microspheres (Life Technologies, 1:1000 in 0.01% poly-L-lysine in PBS) were added as fiducials markers shortly before imaging. The dSTORM buffer consisted of 10% D-glucose (v/v), 10 mM MEA, 50  $\mu$ g/ml glucose oxidase, and 4  $\mu$ g/ml catalase, pH 7.4, in PBS. For each reconstructed image, a series of 20,000 to 50,000 images were taken at 50 Hz. Event density was kept constant by adjusting the illumination at 405 nm. Image reconstruction and drift correction were performed using RapidStorm (70). The optical resolution was estimated using the Fourier Ring Correlation supplied by RapidStorm. HEF cluster size was analyzed by Voronoi tessellation using ClusterVisu (36). Only clusters with a diameter >100 nm were included in the subsequent analysis.

### Flow cytometry to analyze surface transport of HEF

To quantify surface transport of HEF in transfected HEK-293T cells, total and surface fluorescence intensities of HEF were determined by flow cytometry. HEK-293T cells grown in 6-well plates were transfected with plasmids and incubated for 48 h at 33 °C. Cells were then scraped from the plates and

fixed with 4% formaldehyde for 20 min. For measurement of surface HEF, cells were directly treated with blocking solution (5% BSA) for 45 min. For analysis of total HEF, cells were permeabilized using 0.1% Triton X-100 in PBS for 10 min prior to blocking. Cells were then incubated with primary anti-HEF monoclonal antibody 8J3B4 (1:500) and secondary anti-mouse Alexa Fluor 488 antibody (1:5000, A11001, Invitrogen). Cells transfected with empty vector were used as negative control, and their mean fluorescence intensity was subtracted from the fluorescence from cells expressing HEF. At least 10,000 cells were analyzed for each sample, which were measured with CytoFLEX S (BECKMAN COULTER) and analyzed using FlowJo (Data Analysis Software v10).

### Purification of viruses or protein particles for electron microscopy

HEK-293T grown in 150 mm dishes or MDCK I cells grown in T175 flasks were transfected with 30  $\mu$ g plasmid using Lipofectamine 2000 or infected with an MOI of 0.05. Cell culture supernatants were removed 48 h after transfection or 5 days postinfection and centrifuged at 4000g for 30 min to clear them from cell debris. Released particles or viruses were pelleted at 28,000g for 2 h at 4 °C (Beckman, SW32TI rotor) through a 20% sucrose cushion. The pellets were resuspended in PBS and stored at 4 °C for a maximum of 3 days prior to electron microscopy.

### Cryo-ET of virus particles

For cryo-ET of the viruses, perforated carbon film-covered microscopical 200 mesh grids (R1/4 batch of Quantifoil, MicroTools GmbH) were cleaned with chloroform and hydrophilized by 60 s glow discharging at 8 W in a BALTEC MED 020 device (Leica Microsystems), before 4  $\mu$ l aliquots of the virus solution were applied to the grids. The samples were vitrified by automatic blotting and plunge freezing with a FEI VitroBotMark IV (Thermo Fisher Scientific) using liquid ethane as cryogen. The vitrified specimens were transferred under liquid nitrogen into the autoloader of a FEI TALOS ARCTICA electron microscope (Thermo Fisher Scientific). This microscope is equipped with a high-brightness field-emission gun operated at an acceleration voltage of 200 kV. Single-axis tilt series ( $\pm 64^\circ$  at  $2^\circ$  angular increment) were recorded with the Falcon 3 direct electron detector (Thermo Fisher Scientific) using a Volta Phase Plate at 28 K primary magnification with a total dose lower than 100 e<sup>-</sup>/Å<sup>2</sup>. Tomogram reconstruction was performed using Thermo Fisher InSpec3D software.

### "Negative-stain" transmission electron microscopy of protein particles

Aliquots of protein particle solution (5  $\mu$ l) was absorbed onto hydrophilized carbon-coated collodium film that covered the copper grids (400 mesh). The supernatant fluid was removed by blotting with a filter paper, and the sample was allowed to dry in air. Contrast-enhancing heavy-metal stain solution (1% phosphotungstic acid at pH 7.4) was subsequently

## Influenza C virus budding

applied for 45 s and blotted again. A standard holder was used to transfer the dried samples into a FEI Talos L120C transmission electron microscope (Thermo Fisher Scientific Inc) equipped with a LAB<sub>6</sub> cathode operating at 120 kV or into a Tecnai F20 TEM (Thermo Fisher Scientific Inc) equipped with a field emission gun operating at 160 kV. Micrographs were taken with a FEI Ceta (L120C) or a FEI Eagle (Tecnai) 4k × 4k CCD camera.

### Data availability

All data are contained within the manuscript or in the supporting information.

**Supporting information**—This article contains supporting information.

**Acknowledgments**—We thank Robert Vlasak (University Salzburg, Austria) for his generous gift of the reverse genetics system and HEF antibodies. We would like to acknowledge the assistance of the Core Facility BioSupraMol supported by the DFG.

**Author contributions**—X. Z., T. A., and K. L. investigation; X. Z., T. A., A. H., and K. L. writing-original draft; S. S. and A. H. supervision; S. S. and M. V. funding acquisition; A. H., K. L., and M. V. conceptualization; M. V. writing-reviewing and editing.

**Funding and additional information**—This work was supported by the German Research Foundation (DFG), grant Ve 141/18-1 and SFB 1449 (Dynamic hydrogels at biointerfaces), by the Fundamental Research Funds for the Central Universities (grant No. Y0201900459), The Young Top-Notch Talents of National Ten Thousand Talent Program “Six Talent Peaks Project of Jiangsu Province of China” (grant No. NY-045), the China Scholarship Council fellowship, and the Bioinformatics Center of Nanjing Agricultural University.

**Conflict of interest**—The authors declare that they have no conflicts of interest with the contents of this article.

**Abbreviations**—The abbreviations used are: CHO-K1, Chinese hamster ovary cells; cryo-EM, cryo-electron microscopy; DMEM, Dulbecco’s modified Eagle medium; dSTORM, direct stochastic optical reconstruction microscopy; ER, endoplasmic reticulum; FCS, fetal calf serum; Flu C, influenza C virus; Flu D, influenza D virus; GUVs, giant unilamellar vesicles; HA, hemagglutinin; HEF, hemagglutinin-esterase-fusion glycoprotein; HEK-293T, human embryonic kidney-293T cells; MDCK I, Madin-Darby canine kidney cells subline I; MOI, multiplicity of infection; NA, neuraminidase; PFU, plaque forming unit; TCID<sub>50</sub>, Tissue culture infective dose; VLPs, virus-like particles.

### References

1. Sederdahl, B. K., and Williams, J. V. (2020) Epidemiology and clinical characteristics of influenza C virus. *Viruses* **12**, 89
2. Wolff, T., and Veit, M. (2021) Influenza B, C and D viruses (Orthomyxoviridae). In: Bamford, D. H., Zuckerman, M., eds. *Encyclopedia of Virology*, Academic Press, Cambridge, MA: 561–574
3. Hause, B. M., Ducatez, M., Collin, E. A., Ran, Z., Liu, R., Sheng, Z., Armien, A., Kaplan, B., Chakravarty, S., Hoppe, A. D., Webby, R. J., Simonson, R. R., and Li, F. (2013) Isolation of a novel swine influenza

virus from Oklahoma in 2011 which is distantly related to human influenza C viruses. *PLoS Pathog* **9**, e1003176

4. Su, S., Fu, X., Li, G., Kerlin, F., and Veit, M. (2017) Novel influenza D virus: Epidemiology, pathology, evolution and biological characteristics. *Virulence* **8**, 1580–1591
5. Muraki, Y., and Hongo, S. (2010) The molecular virology and reverse genetics of influenza C virus. *Jpn. J. Infect Dis.* **63**, 157–165
6. Herrler, G., and Klenk, H. D. (1991) Structure and function of the HEF glycoprotein of influenza C virus. *Adv. Virus Res.* **40**, 213–234
7. Wang, M., and Veit, M. (2016) Hemagglutinin-esterase-fusion (HEF) protein of influenza C virus. *Protein Cell* **7**, 28–45
8. Rogers, G. N., Herrler, G., Paulson, J. C., and Klenk, H. D. (1986) Influenza C virus uses 9-O-acetyl-N-acetylneuraminic acid as a high affinity receptor determinant for attachment to cells. *J. Biol. Chem.* **261**, 5947–5951
9. Herrler, G., Rott, R., Klenk, H. D., Muller, H. P., Shukla, A. K., and Schauer, R. (1985) The receptor-destroying enzyme of influenza C virus is neuraminidase-O-acetyltransferase. *EMBO J.* **4**, 1503–1506
10. Nakatsu, S., Murakami, S., Shindo, K., Horimoto, T., Sagara, H., Noda, T., and Kawaoka, Y. (2018) Influenza C and D viruses package eight organized ribonucleoprotein complexes. *J. Virol.* **92**, e02084-17
11. Flewett, T. H., and Apostolov, K. (1967) A reticular structure in the wall of influenza C virus. *J. Gen. Virol.* **1**, 297–304
12. Herrler, G., Nagele, A., Meier-Ewert, H., Bhowm, A. S., and Compans, R. W. (1981) Isolation and structural analysis of influenza C virion glycoproteins. *Virology* **113**, 439–451
13. Rosenthal, P. B., Zhang, X., Formanowski, F., Fitz, W., Wong, C. H., Meier-Ewert, H., Skehel, J. J., and Wiley, D. C. (1998) Structure of the haemagglutinin-esterase-fusion glycoprotein of influenza C virus. *Nature* **396**, 92–96
14. Song, H., Qi, J., Khedri, Z., Diaz, S., Yu, H., Chen, X., Varki, A., Shi, Y., and Gao, G. F. (2016) An open receptor-binding cavity of hemagglutinin-esterase-fusion glycoprotein from newly-identified influenza D virus: Basis for its broad cell tropism. *PLoS Pathog* **12**, e1005411
15. Halldorsson, S., Sader, K., Turner, J., Calder, L. J., and Rosenthal, P. B. (2021) *In situ* structure and organization of the influenza C virus surface glycoprotein. *Nat. Commun.* **12**, 1694
16. Bottcher, C., Ludwig, K., Herrmann, A., van Heel, M., and Stark, H. (1999) Structure of influenza haemagglutinin at neutral and at fusogenic pH by electron cryo-microscopy. *FEBS Lett.* **463**, 255–259
17. Rossman, J. S., and Lamb, R. A. (2011) Influenza virus assembly and budding. *Virology* **411**, 229–236
18. Schmitt, A. P., and Lamb, R. A. (2005) Influenza virus assembly and budding at the viral budzone. *Adv. Virus Res.* **64**, 383–416
19. Welsch, S., Muller, B., and Krausslich, H. G. (2007) More than one door - budding of enveloped viruses through cellular membranes. *FEBS Lett.* **581**, 2089–2097
20. Wang, D., Harmon, A., Jin, J., Francis, D. H., Christopher-Hennings, J., Nelson, E., Montelaro, R. C., and Li, F. (2010) The lack of an inherent membrane targeting signal is responsible for the failure of the matrix (M1) protein of influenza A virus to bud into virus-like particles. *J. Virol.* **84**, 4673–4681
21. Chlanda, P., and Zimmerberg, J. (2016) Protein-lipid interactions critical to replication of the influenza A virus. *FEBS Lett.* **590**, 1940–1954
22. Veit, M., Engel, S., Thaa, B., Scolari, S., and Herrmann, A. (2013) Lipid domain association of influenza virus proteins detected by dynamic fluorescence microscopy techniques. *Cell Microbiol.* **15**, 179–189
23. Chlanda, P., Schraidt, O., Kummer, S., Riches, J., Oberwinkler, H., Prinz, S., Krausslich, H. G., and Briggs, J. A. (2015) Structural analysis of the roles of influenza A virus membrane-associated proteins in assembly and morphology. *J. Virol.* **89**, 8957–8966
24. Bethune, J., and Wieland, F. T. (2018) Assembly of COPI and COPII vesicular coat proteins on membranes. *Annu. Rev. Biophys.* **47**, 63–83
25. Barnard, T. R., Abram, Q. H., Lin, Q. F., Wang, A. B., and Sagan, S. M. (2021) Molecular determinants of flavivirus virion assembly. *Trends Biochem. Sci.* **46**, 378–390

26. Snead, W. T., Hayden, C. C., Gadok, A. K., Zhao, C., Lafer, E. M., Rangamani, P., and Stachowiak, J. C. (2017) Membrane fission by protein crowding. *Proc. Natl. Acad. Sci. U. S. A.* **114**, E3258–E3267
27. Gimenez-Andres, M., Copic, A., and Antony, B. (2018) The many faces of amphipathic helices. *Biomolecules* **8**, 45
28. Rossman, J. S., Jing, X., Leser, G. P., and Lamb, R. A. (2010) Influenza virus M2 protein mediates ESCRT-independent membrane scission. *Cell* **142**, 902–913
29. Pekosz, A., and Lamb, R. A. (1997) The CM2 protein of influenza C virus is an oligomeric integral membrane glycoprotein structurally analogous to influenza A virus M2 and influenza B virus NB proteins. *Virology* **237**, 439–451
30. Stewart, S. M., and Pekosz, A. (2012) The influenza C virus CM2 protein can alter intracellular pH, and its transmembrane domain can substitute for that of the influenza A virus M2 protein and support infectious virus production. *J. Virol.* **86**, 1277–1281
31. Saletti, D., Radzimanowski, J., Effantin, G., Midtvedt, D., Mangenot, S., Weissenhorn, W., Bassereau, P., and Bally, M. (2017) The Matrix protein M1 from influenza C virus induces tubular membrane invaginations in an *in vitro* cell membrane model. *Sci. Rep.* **7**, 40801
32. Muraki, Y., Murata, T., Takashita, E., Matsuzaki, Y., Sugawara, K., and Hongo, S. (2007) A mutation on influenza C virus M1 protein affects virion morphology by altering the membrane affinity of the protein. *J. Virol.* **81**, 8766–8773
33. Muraki, Y., Washioka, H., Sugawara, K., Matsuzaki, Y., Takashita, E., and Hongo, S. (2004) Identification of an amino acid residue on influenza C virus M1 protein responsible for formation of the cord-like structures of the virus. *J. Gen. Virol.* **85**, 1885–1893
34. Thaa, B., Herrmann, A., and Veit, M. (2009) The polybasic region is not essential for membrane binding of the matrix protein M1 of influenza virus. *Virology* **383**, 150–155
35. Ye, Z., Robinson, D., and Wagner, R. R. (1995) Nucleus-targeting domain of the matrix protein (M1) of influenza virus. *J. Virol.* **69**, 1964–1970
36. Andronov, L., Orlov, I., Lutz, Y., Vonesch, J. L., and Klaholz, B. P. (2016) ClusterViSu, a method for clustering of protein complexes by Voronoi tessellation in super-resolution microscopy. *Sci. Rep.* **6**, 24084
37. Hongo, S., Sugawara, K., Nishimura, H., Muraki, Y., Kitame, F., and Nakamura, K. (1994) Identification of a second protein encoded by influenza C virus RNA segment 6. *J. Gen. Virol.* **75**, 3503–3510
38. Chen, B. J., Leser, G. P., Morita, E., and Lamb, R. A. (2007) Influenza virus hemagglutinin and neuraminidase, but not the matrix protein, are required for assembly and budding of plasmid-derived virus-like particles. *J. Virol.* **81**, 7111–7123
39. Veit, M., Reverey, H., and Schmidt, M. F. (1996) Cytoplasmic tail length influences fatty acid selection for acylation of viral glycoproteins. *Biochem. J.* **318**, 163–172
40. Crescenzo-Chaigne, B., and van der Werf, S. (2007) Rescue of influenza C virus from recombinant DNA. *J. Virol.* **81**, 11282–11289
41. O'Callaghan, R. J., Loughlin, M., Labat, D. D., and Howe, C. (1977) Properties of influenza C virus grown in cell culture. *J. Virol.* **24**, 875–882
42. Wang, M., Ludwig, K., Bottcher, C., and Veit, M. (2016) The role of stearate attachment to the hemagglutinin-esterase-fusion glycoprotein HEF of influenza C virus. *Cell Microbiol.* **18**, 692–704
43. Jin, H., Leser, G. P., Zhang, J., and Lamb, R. A. (1997) Influenza virus hemagglutinin and neuraminidase cytoplasmic tails control particle shape. *EMBO J.* **16**, 1236–1247
44. Takashita, E., Muraki, Y., Sugawara, K., Asao, H., Nishimura, H., Suzuki, K., Tsuji, T., Hongo, S., Ohara, Y., Kawaoka, Y., Ozawa, M., and Matsuzaki, Y. (2012) Intrinsic temperature sensitivity of influenza C virus hemagglutinin-esterase-fusion protein. *J. Virol.* **86**, 13108–13111
45. Hongo, S., Sugawara, K., Muraki, Y., Kitame, F., and Nakamura, K. (1997) Characterization of a second protein (CM2) encoded by RNA segment 6 of influenza C virus. *J. Virol.* **71**, 2786–2792
46. Lamb, R. A., Zebedee, S. L., and Richardson, C. D. (1985) Influenza virus M2 protein is an integral membrane protein expressed on the infected-cell surface. *Cell* **40**, 627–633
47. Sharma, M., Yi, M., Dong, H., Qin, H., Peterson, E., Busath, D. D., Zhou, H. X., and Cross, T. A. (2010) Insight into the mechanism of the influenza A proton channel from a structure in a lipid bilayer. *Science* **330**, 509–512
48. Hu, B., Siche, S., Moller, L., and Veit, M. (2020) Amphipathic helices of cellular proteins can replace the helix in M2 of influenza A virus with only small effects on virus replication. *J. Virol.* **94**, e01605-19
49. Rossman, J. S., Jing, X., Leser, G. P., Balannik, V., Pinto, L. H., and Lamb, R. A. (2010) Influenza virus m2 ion channel protein is necessary for filamentous virion formation. *J. Virol.* **84**, 5078–5088
50. Stewart, S. M., and Pekosz, A. (2011) Mutations in the membrane-proximal region of the influenza A virus M2 protein cytoplasmic tail have modest effects on virus replication. *J. Virol.* **85**, 12179–12187
51. Wang, J., Pielak, R. M., McClintock, M. A., and Chou, J. J. (2009) Solution structure and functional analysis of the influenza B proton channel. *Nat. Struct. Mol. Biol.* **16**, 1267–1271
52. Martin, K., and Helenius, A. (1991) Nuclear transport of influenza virus ribonucleoproteins: The viral matrix protein (M1) promotes export and inhibits import. *Cell* **67**, 117–130
53. Sugawara, K., Nishimura, H., Hongo, S., Kitame, F., and Nakamura, K. (1991) Antigenic characterization of the nucleoprotein and matrix protein of influenza C virus with monoclonal antibodies. *J. Gen. Virol.* **72**, 103–109
54. Cao, S., Jiang, J., Li, J., Li, Y., Yang, L., Wang, S., Yan, J., Gao, G. F., and Liu, W. (2014) Characterization of the nucleocytoplasmic shuttle of the matrix protein of influenza B virus. *J. Virol.* **88**, 7464–7473
55. Cao, S., Liu, X., Yu, M., Li, J., Jia, X., Bi, Y., Sun, L., Gao, G. F., and Liu, W. (2012) A nuclear export signal in the matrix protein of influenza A virus is required for efficient virus replication. *J. Virol.* **86**, 4883–4891
56. Nishimura, H., Hara, M., Sugawara, K., Kitame, F., Takiguchi, K., Umetsu, Y., Tonosaki, A., and Nakamura, K. (1990) Characterization of the cord-like structures emerging from the surface of influenza C virus-infected cells. *Virology* **179**, 179–188
57. Nishimura, H., Hongo, S., Sugawara, K., Muraki, Y., Kitame, F., Washioka, H., Tonosaki, A., and Nakamura, K. (1994) The ability of influenza C virus to generate cord-like structures is influenced by the gene coding for M protein. *Virology* **200**, 140–147
58. Gomez-Puertas, P., Albo, C., Perez-Pastrana, E., Vivo, A., and Portela, A. (2000) Influenza virus matrix protein is the major driving force in virus budding. *J. Virol.* **74**, 11538–11547
59. Dahmani, I., Ludwig, K., and Chiantia, S. (2019) Influenza A matrix protein M1 induces lipid membrane deformation *via* protein multimerization. *Biosci. Rep.* **39**, BSR20191024
60. Hilsch, M., Goldenbogen, B., Sieben, C., Hofer, C. T., Rabe, J. P., Klipp, E., Herrmann, A., and Chiantia, S. (2014) Influenza A matrix protein M1 multimerizes upon binding to lipid membranes. *Biophys. J.* **107**, 912–923
61. Arzt, S., Baudin, F., Barge, A., Timmins, P., Burmeister, W. P., and Rui-grok, R. W. (2001) Combined results from solution studies on intact influenza virus M1 protein and from a new crystal form of its N-terminal domain show that M1 is an elongated monomer. *Virology* **279**, 439–446
62. Peukes, J., Xiong, X., Erendsson, S., Qu, K., Wan, W., Calder, L. J., Schraidt, O., Kummer, S., Freund, S. M. V., Krausslich, H. G., and Briggs, J. A. G. (2020) The native structure of the assembled matrix protein 1 of influenza A virus. *Nature* **587**, 495–498
63. Hofer, C. T., Di Lella, S., Dahmani, I., Jungnick, N., Bordag, N., Bobone, S., Huang, Q., Keller, S., Herrmann, A., and Chiantia, S. (2019) Structural determinants of the interaction between influenza A virus matrix protein M1 and lipid membranes. *Biochim. Biophys. Acta Biomembr.* **1861**, 1123–1134
64. Jumper, J., Evans, R., Pritzel, A., Green, T., Figurnov, M., Ronneberger, O., Tunyasuvunakool, K., Bates, R., Zidek, A., Potapenko, A., Bridgland, A., Meyer, C., Kohl, S. A. A., Ballard, A. J., Cowie, A., *et al.* (2021) Highly accurate protein structure prediction with AlphaFold. *Nature* **596**, 583–589
65. Zhang, J., Pekosz, A., and Lamb, R. A. (2000) Influenza virus assembly and lipid raft microdomains: A role for the cytoplasmic tails of the spike glycoproteins. *J. Virol.* **74**, 4634–4644
66. Ellgaard, L., and Helenius, A. (2003) Quality control in the endoplasmic reticulum. *Nat. Rev. Mol. Cell Biol.* **4**, 181–191

## Influenza C virus budding

67. Yondola, M. A., Fernandes, F., Belicha-Villanueva, A., Uccellini, M., Gao, Q., Carter, C., and Palese, P. (2011) Budding capability of the influenza virus neuraminidase can be modulated by tetherin. *J. Virol.* **85**, 2480–2491
68. Pachler, K., Mayr, J., and Vlasak, R. (2010) A seven plasmid-based system for the rescue of influenza C virus. *J. Mol. Genet. Med.* **4**, 239–246
69. van de Linde, S., Loschberger, A., Klein, T., Heidebreder, M., Wolter, S., Heilemann, M., and Sauer, M. (2011) Direct stochastic optical reconstruction microscopy with standard fluorescent probes. *Nat. Protoc.* **6**, 991–1009
70. Wolter, S., Loschberger, A., Holm, T., Aufmkolk, S., Dabauvalle, M. C., van de Linde, S., and Sauer, M. (2012) rapidSTORM: Accurate, fast open-source software for localization microscopy. *Nat. Methods* **9**, 1040–1041